nature chemical biology

ARTICLES

https://doi.org/10.1038/s41589-020-0533-x

Check for updates

A small molecule G6PD inhibitor reveals immune dependence on pentose phosphate pathway

Jonathan M. Ghergurovich[1,2,10], Juan C. García-Cañaveras[1,3,10], Joshua Wang[3], Emily Schmidt[1,3], Zhaoyue Zhang[1,3], Tara TeSlaa[1,3], Harshel Patel[1,3], Li Chen[1,3], Emily C. Britt[4], Marta Piqueras-Nebot[5], Mari Carmen Gomez-Cabrera[6,7], Agustín Lahoz[5], Jing Fan[4], Ulf H. Beier[8], Hahn Kim[3,9] and Joshua D. Rabinowitz[1,3] ✉

Glucose is catabolized by two fundamental pathways, glycolysis to make ATP and the oxidative pentose phosphate pathway to make reduced nicotinamide adenine dinucleotide phosphate (NADPH). The first step of the oxidative pentose phosphate pathway is catalyzed by the enzyme glucose-6-phosphate dehydrogenase (G6PD). Here we develop metabolite reporter and deuterium tracer assays to monitor cellular G6PD activity. Using these, we show that the most widely cited G6PD antagonist, dehydroepiandosterone, does not robustly inhibit G6PD in cells. We then identify a small molecule (G6PDi-1) that more effectively inhibits G6PD. Across a range of cultured cells, G6PDi-1 depletes NADPH most strongly in lymphocytes. In T cells but not macrophages, G6PDi-1 markedly decreases inflammatory cytokine production. In neutrophils, it suppresses respiratory burst. Thus, we provide a cell-active small molecule tool for oxidative pentose phosphate pathway inhibition, and use it to identify G6PD as a pharmacological target for modulating immune response.

Across all forms of life, the redox cofactor reduced nicotinamide adenine dinucleotide phosphate (NADPH) donates high-energy electrons for reductive biosynthesis and antioxidant defense[1]. The critical nature of these processes requires effective maintenance of the levels of NADPH and its redox partner $NADP^+$. In the cytosol of mammalian cells, reduction of $NADP^+$ to NADPH mainly occurs via three routes: malic enzyme 1 (ME1), isocitrate dehydrogenase 1 (IDH1) and the oxidative pentose phosphate pathway (oxPPP)[2]. While ME1 and IDH1 extract hydrides from the citric acid-cycle-derived metabolites, the oxPPP diverts glucose-6-phospate from glycolysis to generate two equivalents of NADPH; one by glucose-6-phosphate dehydrogenase (G6PD), which catalyzes the first and committed step, and one by 6-phosphogluconate dehydrogenase (PGD).

G6PD is ubiquitously expressed in mammalian tissues, with highest expression in immune cells and testes[3]. It is also often upregulated in tumors[4–7]. Genetically, G6PD knockout mice are inviable[8]. Nevertheless, G6PD hypomorphic alleles are common in humans, affecting roughly one in 20 people worldwide[9]. These mutations provide protection from malaria, but sensitize mature red blood cells (RBCs) to oxidative stressors. The vulnerability of RBCs to mutant G6PD may reflect RBCs' lack of mitochondria and thus inability to endogenously produce the substrates of ME1 or IDH1. Alternatively, it may reflect RBCs' lack of nuclei and thus inability to replace the mutant G6PD protein as the cells age. In other tissues, the function of G6PD is less investigated. Using a genetic approach, we recently showed that cancer cell lines lacking G6PD have elevated $NADP^+$ levels, but are nevertheless able to proliferate and maintain NADPH pools through compensatory ME1 and/or IDH1 flux[10]. Whether nontransformed cells are similarly flexible remains unclear.

Potent and selective small molecule inhibitors are useful tools for studying the function of metabolic enzymes. So far, several small molecule inhibitors of G6PD have been described[11–13], most notably the steroid derivative dehydroepiandosterone (DHEA) (**1**) (Fig. 1a). First reported in 1960, DHEA binds mammalian G6PD uncompetitively against both reaction substrates[14]. Since then, DHEA and its derivatives have been used as G6PD inhibitors in hundreds of studies, including a variety of in vitro and in vivo cancer settings where they display antiproliferative activity[15–17]. However, these readouts of cellular activity are indirect, and it has been proposed that the effects of DHEA may arise from alternative mechanisms other than G6PD inhibition[15,18].

To properly evaluate cellular target engagement, it is important to use assays that specifically monitor the reaction of interest[19–21]. However, developing assays that monitor NADPH-producing reactions can be particularly challenging, since NADPH is difficult to measure[22] and is produced by multiple pathways (where inhibition of one can be masked by compensatory production from others).

Here, we develop G6PD cellular target engagement assays and use them to show that DHEA, even at high doses, minimally inhibits G6PD in cells. We then identify a nonsteroidal small molecule inhibitor of G6PD, G6PDi-1 (**2**), which demonstrates on-target reversible cellular activity against G6PD. Use of G6PDi-1 across a wide range of mammalian cells revealed that immune cells,

[1]Lewis Sigler Institute for Integrative Genomics, Princeton University, Princeton, NJ, USA. [2]Department of Molecular Biology, Princeton University, Princeton, NJ, USA. [3]Department of Chemistry, Princeton University, Princeton, NJ, USA. [4]Morgridge Institute for Research, Department of Nutritional Sciences, University of Wisconsin-Madison, Madison, WI, USA. [5]Biomarkers and Precision Medicine Unit, Instituto de Investigación Sanitaria Fundación Hospital La Fe, Valencia, Spain. [6]Freshage Research Group, Department of Physiology, Faculty of Medicine, University of Valencia, Valencia, Spain. [7]Centro de Investigación Biomédica en Red Fragilidad y Envejecimiento Saludable, Fundación Investigación Hospital Clínico Universitario/INCLIVA, Valencia, Spain. [8]Division of Nephrology, Department of Pediatrics, Children's Hospital of Philadelphia, University of Pennsylvania, Philadelphia, PA, USA. [9]Princeton University Small Molecule Screening Center, Princeton University, Princeton, NJ, USA. [10]These authors contributed equally: Jonathan M. Ghergurovich, Juan C. García-Cañaveras. ✉e-mail: joshr@princeton.edu

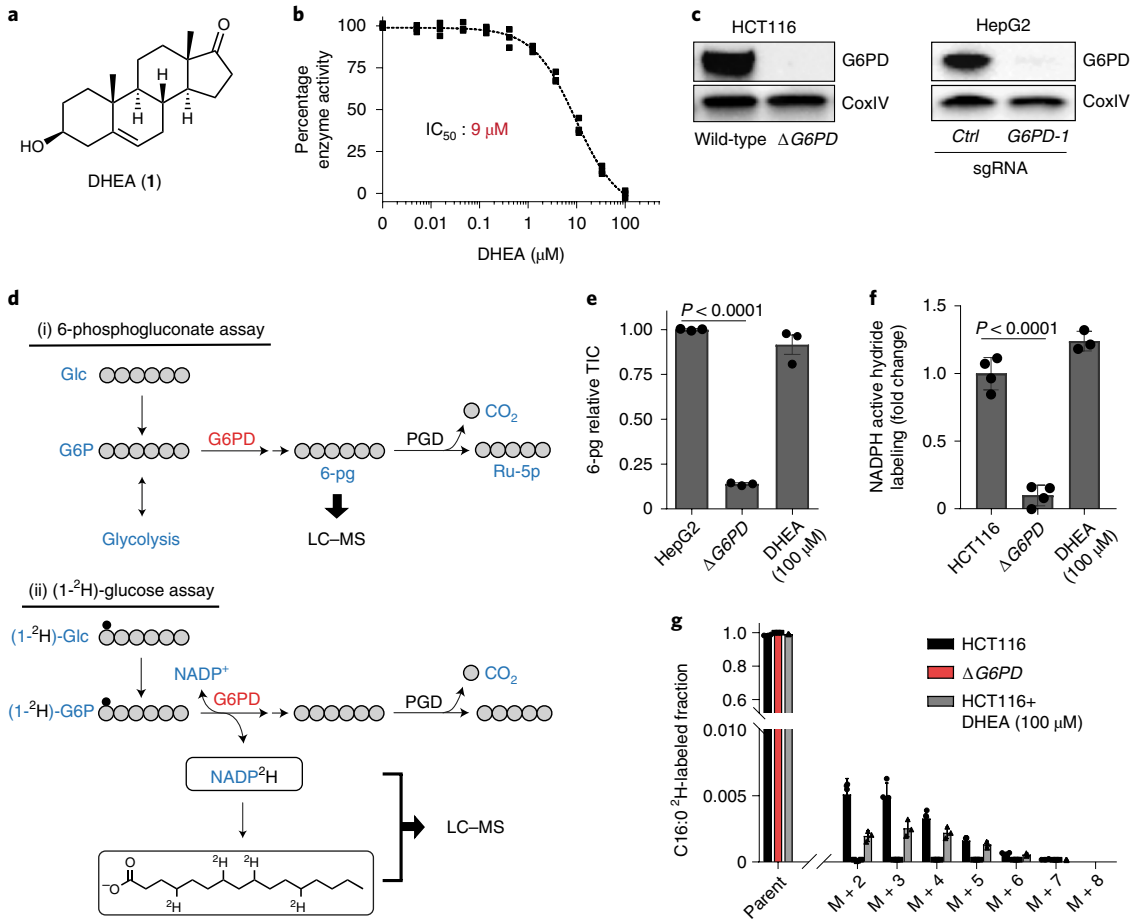

Fig. 1 | Cellular target engagement assays reveal lack of effective G6PD inhibition by DHEA. a, Chemical structure of the steroid derivative DHEA. **b**, In vitro activity of DHEA against recombinant human G6PD ($n=3$). **c**, Western blots of G6PD knockout cells generated using CRISPR–Cas9 (HCT116 knockout is clonal; HepG2 is batch; *Ctrl* represents an intergenic control). See Supplementary Fig. 16 for uncropped gels. Representative results of two independent experiments. sgRNA, single-guide RNA. **d**, Assays for G6PD cellular activity: (i) 6-phosphogluconate (6-pg) levels in HepG2 cells, (ii) deuterium (^{2}H, small black circle) incorporation into NADPH and free palmitic acid from [1-^{2}H]-glucose in HCT116 cells. **e**–**g**, DHEA (100 μM, 2 h) does not phenocopy G6PD knockout (TIC, total ion count by LC–MS; for **e**, HepG2 and Δ*G6PD* refer to sg*Ctrl* and sg*G6PD-1* from **c**, respectively) (mean ± s.d., $n \geq 3$). *P* value calculated using a two-tailed unpaired Student's *t*-test.

especially T cells, are reliant on G6PD for maintaining NADPH levels and effector function.

Results

DHEA does not inhibit G6PD in cell-based assays. To examine the biochemical activity of G6PD, we established a coupled enzymatic assay using recombinant human enzyme (Supplementary Fig. 1a,b). Consistent with previous reports, DHEA demonstrated dose-dependent inhibition of G6PD, with a calculated half-maximal inhibitory constant (IC_{50}) of 9 μM (Fig. 1b)[23].

To assess whether DHEA effectively targets G6PD also in cells, we compared metabolomics of clonally isolated G6PD knockout cells (Δ*G6PD*) (Fig. 1c) with parental HCT116 cells treated with high dose DHEA (100 μM). Global metabolomics showed DHEA treatment did not mirror G6PD knockout (Supplementary Fig. 2a). DHEA failed to deplete the key downstream oxPPP intermediate 6-phosphogluconate (6-pg) (Supplementary Fig. 2b), although measurement was challenging due to low 6-pg levels in this cell line. Through analysis of diverse cell lines, we found that the hepatocellular carcinoma line HepG2 possesses sufficient 6-pg for reliable monitoring of G6PD cellular target engagement (Fig. 1d). In addition, through CRISPR manipulation of 6-phosphogluconate dehydrogenase in HCT116 cells, we identified a hypomorphic cell line (m*PGD*) that builds up 6-pg, facilitating assessment of G6PD target engagement (Supplementary Fig. 3a–c). In m*PGD* HCT116 cells, DHEA (100 μM) modestly suppressed 6-pg (Supplementary Fig. 3d). In HepG2 cells, G6PD knockout (Fig. 1c) substantially decreased 6-pg, whereas DHEA had no effect (Fig. 1e). Together, these observations suggest that DHEA may not consistently and effectively block cellular G6PD.

We next aimed to directly monitor G6PD mediated hydride transfer to NADPH. Specifically, we traced the transfer of deuterium from [1-^{2}H]-glucose, via glucose-6-phosphate, to the NADPH's active hydride (Fig. 1d)[24]. Consistent with this labeling arising primarily from the G6PD reaction, Δ*G6PD* cells demonstrated a nearly complete loss of active hydride labeling (Fig. 1f). The affected step was G6PD, as no change in substrate (G6P) labeling was observed (Supplementary Fig. 2c). A main use of cytosolic NADPH is fat synthesis. We quantified transfer of ^{2}H from glucose via NADPH into palmitate (C16:0), which requires two NADPH per two-carbon unit addition during its synthesis (Fig. 1d)[24]. Near complete loss of labeling into C16:0 from [1-^{2}H]-glucose (Fig. 1g) was observed in Δ*G6PD* cells. DHEA, however, did not decrease either NADPH active hydride labeling (Fig. 1f) or C16:0 labeling (Fig. 1g). Thus, DHEA does not robustly inhibit cellular G6PD.

To evaluate other purported inhibitors of G6PD, we obtained two recently identified small molecules, CB-83 (**3**)[12] and polydatin (**4**)[13] (Supplementary Fig. 4a). Like DHEA, both CB-83 and polydatin display antiproliferative effects against transformed cells, but direct evidence of cellular G6PD inhibition is lacking[12,13]. At a dose higher than that reported to impair cell growth[13], polydatin failed to decrease 6-pg levels (Supplementary Fig. 4b) or NADPH active hydride labeling (Supplementary Fig. 4c), consistent with lack of cellular target engagement of G6PD. Although individual experimental results were variable, CB-83 appeared to augment G6PD activity (Supplementary Fig. 4b,c). This could potentially reflect CB-83 activating the oxPPP by inducing oxidative stress. Despite this complexity, like DHEA, these compounds do not appear to be cell-active G6PD inhibitors.

G6PDi-1, a nonsteroidal, cell-active inhibitor of G6PD. We combed the literature for a compound series that could serve as a suitable chemical starting point for inhibitor discovery. Our search identified a nonsteroidal aminoquinazolinone series that was recently discovered and optimized against *Trypanosoma cruzi* G6PD[25]. Synthesis of representative compounds identified G6PDi-precursor (**5**) with low micromolar in vitro activity against human G6PD (Fig. 2a,b). Successive rounds of optimization led to replacement of the aminophenyl ring with a cyano-thiophene and expansion of the alkyl quinazolinone region by one methylene, ultimately identifying G6PDi-1, a submicromolar inhibitor of human G6PD ($IC_{50} = 0.07\,\mu M$). Additionally, we identified a structural analog (designated G6PDi-*neg-ctrl*, **6**) that lacked any activity against G6PD to serve as a negative control compound (Fig. 2a,b). In vitro activities were verified in an orthogonal, liquid chromatography–mass spectrometry (LC–MS) assay that monitors 6-pg production by recombinant human G6PD (Supplementary Fig. 5a). Follow up in vitro dilution experiments (Supplementary Fig. 5b) and competition assays against both substrates (Supplementary Fig. 5c) showed G6PDi-1 binds to G6PD reversibly and noncompetitively. Cellular thermal shift assay (CETSA) using HepG2 lysates demonstrated substantial thermal stabilization of G6PD by G6PDi-1, but not DHEA up to 56 °C (Supplementary Fig. 6a–c). These data collectively support a reversible direct physical interaction between G6PDi-1 and G6PD at an allosteric site, with G6PDi-1 binding inhibiting enzyme catalytic activity.

To investigate cellular target engagement, G6PDi-1 was evaluated by metabolomics in wild-type and Δ*G6PD* HCT116 cells (Supplementary Fig. 7) and in our established target engagement assays. The metabolomics revealed some potential off-target effects on purine nucleosides. Nevertheless, there was clear cellular target engagement. In HepG2 cells, treatment with G6PDi-1, but not G6PDi-*neg-ctrl* or DHEA, led to a dose-dependent decrease in 6-pg levels ($IC_{50} \approx 13\,\mu M$, Fig. 2c). Similarly, 6-pg levels in m*PGD* HCT116 cells were much more effectively suppressed by G6PDi-1 than DHEA (Supplementary Fig. 8a). Consistent with this effect arising from reversible binding of G6PD, 6-pg levels completely recovered within 2 h of removing the inhibitor (Fig. 2d). Additionally, treatment of HCT116 cells with G6PDi-1, but not *neg-ctrl* or DHEA, led to a dose-dependent decrease in ^2H transfer from [1-^2H]-glucose to NADPH's active hydride ($IC_{50} \approx 31\,\mu M$, Fig. 2e) and downstream product C16:0 (Fig. 2f). The affected step was G6PD, as no change in G6P labeling was observed (Supplementary Fig. 8b). In addition, as expected for G6PD inhibition, we observed a dose-dependent increase in $NADP^+$/NADPH (Fig. 2g).

To further assess the use of G6PDi-1 as a cellular G6PD inhibitor, we built on previous work that established epithelial cells undergoing matrix detachment are subjected to increased levels of oxidative stress, and are in turn dependent on oxPPP activity for survival[26]. As expected, colony formation of Δ*G6PD* cells is dramatically impaired (Fig. 2h). Consistent with G6PDi-1 possessing cellular G6PD activity, a dose-dependent decrease in colony formation is observed with G6PDi-1, but not G6PDi-*neg-ctrl*, an effect that is rescued by exogenous antioxidants (Fig. 2i). Taken together, these data show that G6PDi-1 is a cell-active G6PD inhibitor.

G6PDi-1 reveals T cell dependence on oxPPP. It was recently established that transformed cells can maintain NADPH levels in the face of G6PD loss by using malic enzyme 1 (ME1) and/or isocitrate dehydrogenase 1 (1DH1) to make NADPH[10]. Indeed, despite effectively penetrating HCT116 and HepG2 cells (Supplementary Fig. 9a) and effectively inhibiting G6PD activity, NADPH pools were largely unperturbed by G6PDi-1 treatment (Supplementary Fig. 9b,c). To evaluate the potential for different cells to acutely compensate for G6PD inhibition, we treated a diversity of primary and transformed cell types with G6PDi-1, reasoning that cells reliant on the oxPPP would be unable to maintain their NADPH pools. As expected, we observed that RBCs were fairly sensitive to G6PDi-1. We were surprised, however, to find that T cell lineages were substantially more strongly affected, manifesting a greater than tenfold decrease in NADPH, accompanied by a corresponding increase in $NADP^+$ (Fig. 3a). Thus, T cells appear to be particularly dependent on the oxPPP for maintaining their NADPH pools.

Since T cell activation involves substantial metabolic rewiring[27], we decided to investigate whether an activation-driven metabolic program determined T cell dependency on the oxPPP. To this end, we isolated naïve $CD8^+$ T cells from mouse spleen and either maintained them in the naïve state by culturing them with IL-7 or activated them with plate-bound αCD3/αCD28 and IL-2. On activation, we observed an increase in G6PD protein, which began within 8 h and became prominent by 24 h (Supplementary Fig. 10a). In line with this observation, absolute oxPPP flux as measured using radioactive CO_2 capture increased by more than tenfold on activation (Fig. 3b).

Consistent with the inability of T cells to maintain NADPH using compensatory pathways, neither naïve nor activated $CD8^+$ T cells possess substantial ME1 or IDH1 (Supplementary Fig. 10a). To complement these enzyme abundance measurements, we used ^2H-tracing to assess the relative contribution from ME1, IDH1 and the oxPPP to cytosolic NADPH[10,24]. Using a combination of five tracers (Supplementary Fig. 10b,c), we found that the oxPPP accounts for nearly all cytosolic NADPH production in $CD8^+$ and $CD4^+$ T cells activated with αCD3/αCD28 and IL-2, but not in naïve $CD8^+$ and $CD4^+$ T cells maintained in IL-7 supplemented media (Fig. 3c and Supplementary Fig. 10d).

To examine further the impact of G6PDi-1, mouse $CD8^+$ and $CD4^+$ T cells at day 4–5 postactivation were treated with increasing G6PDi-1 in the presence of [1-^2H]-glucose. G6PDi-1 (10 μM) completely blocked ^2H transfer from glucose to NADPH (Fig. 3d and Supplementary Fig. 10e) and decreased NADPH and 6-pg levels (Supplementary Fig. 11a). Similarly, treatment with G6PDi-1 blocked absolute oxPPP flux (Fig. 3e). Consistent with their lower G6PD expression and flux and NADPH requirements for biosynthesis, naïve $CD8^+$T cells were less sensitive to G6PDi-1 than activated $CD8^+$T cells (Supplementary Fig. 10f,g). In activated $CD8^+$ T cells, NADPH, $NADP^+$ and 6-pg levels were restored within 2 h of removing the inhibitor (Fig. 3f and Supplementary Fig. 11b). The effects on NADPH labeling (from [1-^2H]-glucose), and $NADP^+$, NADPH and 6-pg levels occurred within 10 min of G6PDi-1 treatment (Supplementary Fig. 11c). Absolute quantitation of $NADP^+$ and NADPH revealed that the decrease in NADPH concentration induced by G6PDi-1 is matched by an increase in $NADP^+$ concentration, with the total NADP(H) remaining around ~200 μM (Fig. 3g). Collectively, these data confirm that G6PDi-1 is a rapid, reversible G6PD inhibitor that increases the $NADP^+$/NADPH ratio in T cells.

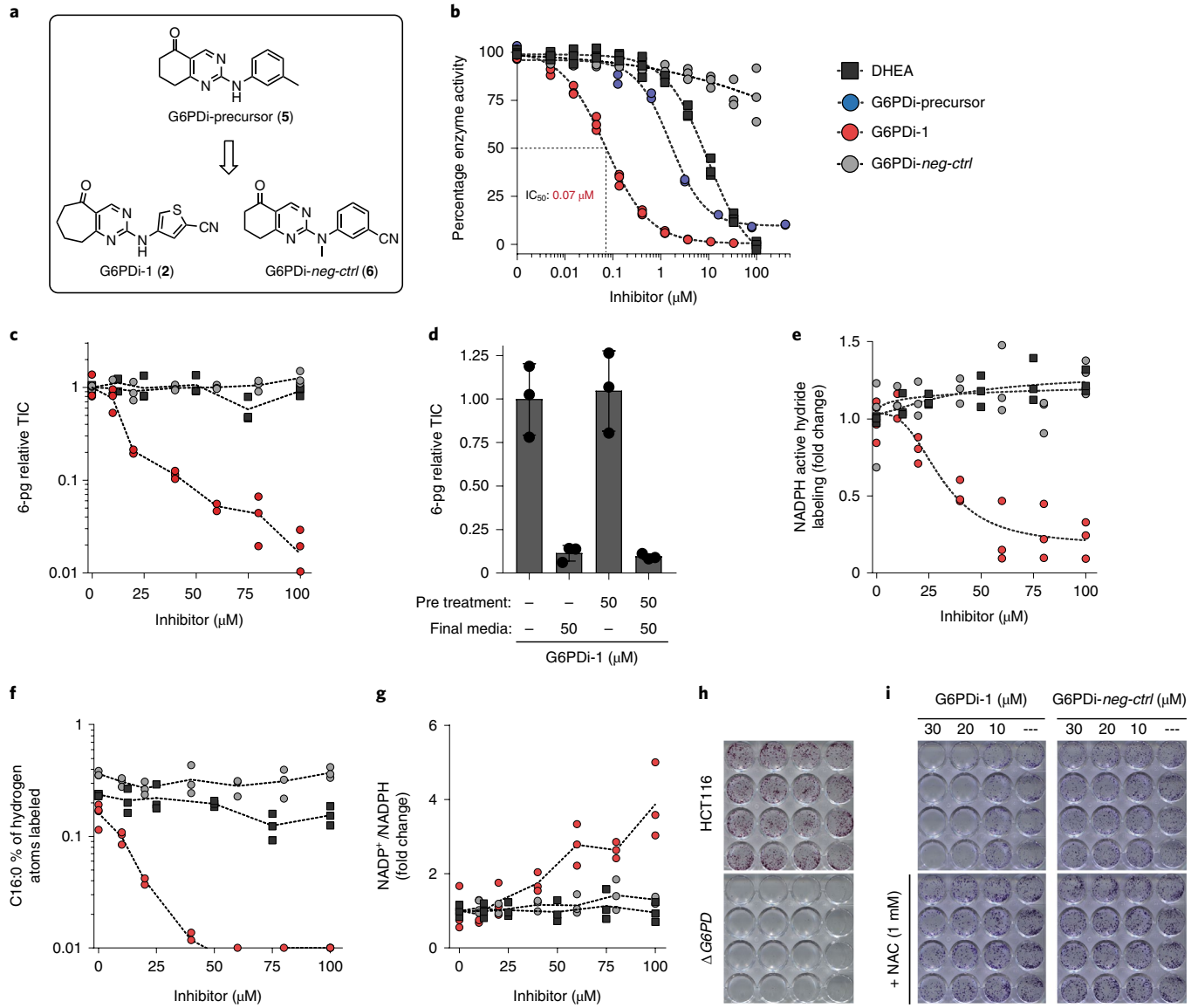

Fig. 2 | A nonsteroidal, cell-active inhibitor of G6PD. a, Chemical structures. **b**, In vitro dose–response curves ($n=3$). **c**, 6-pg dose–response curves (HepG2 cells) ($n=3$). **d**, Reversibility of the cellular activity of G6PDi-1. HepG2 cells were pretreated with indicated media for 2 h, followed by incubation with final media for 2 h (mean ± s.d., $n=3$). **e**, NADPH active hydride ^{2}H-labeling dose–response curves (HCT116 cells, [1-^{2}H]-glucose tracer) ($n=3$). **f**, Free palmitic acid ^{2}H-labeling dose–response curves (HCT116 cells, [1-^{2}H]-glucose tracer) ($n=3$). **g**, NADP$^+$/NADPH ratio dose–response curves (HCT116 cells) ($n=3$). **h**, Representative crystal violet staining of colonies formed from wild-type and Δ*G6PD* HCT116 cells. **i**, Colony formation of HCT116 cells treated with increasing doses of G6PDi-1 and G6PDi-*neg-ctrl*. Representative results of three independent experiments. NAC, *N*-acetylcysteine.

To assess the specificity of the metabolic effects of G6PDi-1, we performed untargeted metabolomics on CD8$^+$ T cells. The greatest metabolite concentration change occurred directly in the substrates and products of G6PD (NADPH, NADP$^+$, 6-pg) and folate metabolites known to be perturbed by G6PD activity loss (dUMP, GAR) (Fig. 3h and Supplementary Fig. 2a)[10]. Thus, G6PDi-1 has clean on-target activity in T cells. Isotope tracing with [U-^{13}C]-glucose and [U-^{13}C]-glutamine revealed that G6PDi-1 decreased the glucose contribution to the citric acid cycle (with a corresponding increase in glutamine contribution) (Supplementary Fig. 12a–l). In addition, fatty acid synthesis, a main consumer of cytosolic NADPH, was nearly completely ablated (Supplementary Fig. 12m). Consistent with the importance of NADPH in controlling oxidative stress, G6PDi-1 treatment elevated reactive oxygen species (ROS) in both CD8$^+$ and CD4$^+$ T cells (Supplementary Fig. 11d). These effects were largely rescued by *N*-acetyl cysteine (Supplementary Fig. 11e).

Recently, a transgenic mouse strain that over-expresses human G6PD (G6PD-Tg) was reported[28] (Fig. 3i). To validate the dependence of T cell NADPH pools on G6PD, CD8$^+$ T cells from G6PD-Tg mice and littermate controls at day 4–5 postactivation were treated with increasing doses of G6PDi-1. G6PD overexpression markedly shifted the dose response to G6PDi-1, rescuing its effects on NADPH and NADP$^+$ (Fig. 3j–k). Thus, G6PDi-1 modulates T cell NADPH by inhibiting G6PD, with introduction of exogenous G6PD activity rescuing T cell redox state.

G6PDi-1 blocks T cell cytokine production. We next explored the functional consequences of oxPPP inhibition using G6PDi-1 in T cells. To test the effect of G6PDi-1 on activation and proliferation, naïve CD8$^+$ T cells were isolated from spleen and activated in vitro with plate-bound αCD3/αCD28 and IL-2. Activation was evaluated by flow cytometry analysis of surface markers CD69

(levels rapidly rise on activation) and CD25 (usually peaking at 24–48 h post-activation), and cell size, which increases over the first 24 h postactivation. To quantify proliferation, naïve cells were stained with CellTrace Violet (CTV) and dye dilution was measured by flow cytometry at day 4 postactivation. Consistent with the late upregulation of oxPPP during activation[29,30] (Supplementary Fig. 10a), G6PDi-1 did not alter the normal upregulation of activation markers or activation-dependent increase in cell size (Fig. 4a). G6PDi-1 had a minimal effect in activation-dependent proliferation (Fig. 4b and Supplementary Fig. 13a) and viability (Supplementary Fig. 13b). G6PDi-1 had also a minimal effect on the proliferation of $CD4^+$ T cells (Supplementary Fig. 13c).

To assess the effect of G6PD inhibition in T cell function, active $CD8^+$ or $CD4^+$ cells were stimulated with phorbol 12-myristate 13-acetate (PMA) and ionomycin in the presence of increasing doses of G6PDi-1 and cytokine production was monitored by intracellular flow cytometry. G6PD inhibition blocked IFNγ and TNFα production in $CD8^+$ and IL-2 and TNFα $CD4^+$ T cells (Fig. 4c and Supplementary Fig. 13d,e).

Proper T cell activation requires ROS signaling while avoiding ROS toxicity[31–33]. Accordingly, we attempted to rescue $CD8^+$ T cell cytokine secretion with the antioxidant *N*-acetyl-cysteine (Supplementary Fig. 13f) or by providing an external source of peroxide/superoxide (Supplementary Fig. 13g), but neither was effective. To confirm that the defect is at the level of signaling, rather than protein synthesis, we examined IFNγ messenger RNA, finding that its levels were also decreased (Fig. 4d). Indeed, signaling during the first hour after restimulation seems to be particularly important, as delayed addition of G6PDi-1 enabled substantial cytokine production to occur (Supplementary Fig. 13h). Restoration of intracellular NADPH levels by transgenic G6PD expression decreased sensitivity to G6PDi-1 and partially normalized both protein and mRNA levels on G6PDi-1 addition (Fig. 4c,d). Thus, G6PD activity is required to maintain proper $NADP^+$/NADPH homeostasis in activated T cells, in a manner that is not readily compensated by generic oxidant or antioxidant, and loss of such homeostasis inhibits T cell effector function.

We next sought to evaluate whether G6PD inhibition impacted the development, proliferation or suppressor function of $CD4^+$ regulatory T cells (T_{reg}). Stimulation with CD3/CD28 in the presence of TGFβ resulted in $Foxp3^+$ cells, whose formation and proliferation were unaffected by G6PDi-1 (Supplementary Fig. 14a–c). Similarly, $CD4^+CD25^+$ T_{reg} cells proliferated and were effective in suppressing the proliferation of conventional $CD4^+$ $CD25^-$ T cells irrespective of G6PDi-1 treatment (Supplementary Fig. 14d–e). Collectively, these data show that, without overtly impacting proliferation or suppressor function, G6PDi-1 inhibits pro-inflammatory cytokine production from activated T cells.

G6PDi-1 suppresses oxidative burst in neutrophils. Motivated by the key role of G6PD in effector function in $CD4^+$ and $CD8^+$ T cells, we decided to evaluate whether the function of other immune cells depends on G6PD activity. In macrophages, G6PDi-1 did not decrease NADPH (Fig. 3a) or lipopolysaccharide (LPS)-induced pro-inflammatory cytokine production or iNOS upregulation (Fig. 5a). Thus, while in T cells G6PD activity is essential for cytokine production, it is dispensable in the case of LPS-stimulated macrophages (Fig. 5b).

In neutrophils, G6PDi-1 did affect NADPH, albeit to a lesser extent than in T cells (Fig. 3a). A key function of neutrophils is ROS generation by NADPH oxidase[34], which requires NADPH and oxygen as substrates. To test the role for the oxPPP in this effector function, mouse and human neutrophils were stimulated with PMA in the presence of 50 μM G6PDi-1 or vehicle control, and oxygen consumption rate (OCR) was used to readout oxidative burst. G6PDi-1 decreased oxidative burst in both mouse and human neutrophils (Fig. 5c,d). Thus, G6PD activity is essential in providing NADPH for ROS generation by NADPH oxidase in neutrophils.

Discussion

Small molecule inhibitors with specific on-target activity are key tools for biological research. Unfortunately, however, many tool compounds fail to robustly engage their targets and/or have extensive off-target effects. Here, we show that the commonly used G6PD inhibitor DHEA, despite clear inhibition of purified enzyme, lacks robust on-target cellular activity at doses above those needed to exhibit antiproliferative effects. Others have previously raised doubts about DHEA's cellular G6PD activity[18], but it has continued to be widely used as a G6PD inhibitor, in part because of evidence that it induces oxidative stress[35]. This, however, is a nonspecific outcome, and in the case of DHEA (and several other recently published 'G6PD inhibitors') may occur unrelated to G6PD target engagement.

Fig. 3 | G6PDi-1 reveals T cells depend on oxPPP for maintaining cellular NADPH. a, LC–MS quantification of NADPH and $NADP^+$ pools across a variety of normal and transformed cell types in response to G6PDi-1 (mean ± s.d., $n = 6$ for RBC, $CD4^+$ and $CD8^+$ T cells, $n = 3$ for the rest of cells). TIC, total ion count. Cell names in red are T cell lineage, blue are cell lines derived from solid tumors. Abbreviations are 2871-8, lung adenocarcinoma (mouse); A549, lung adenocarcinoma (human); L929, fibroblast (mouse); HCT116, colorectal carcinoma (human); iBMK, immortalized baby kidney epithelial (mouse); MΦ, mouse bone-marrow-derived macrophages; unstimulated (MΦ-0), stimulated with LPS + IFNγ (MΦ-1), stimulated with IL-4 (MΦ-2); LNCaP, prostate adenocarcinoma (human); HepG2, hepatocellular carcinoma (human); C2C12, immortalized myoblasts (mouse); HFF, fibroblasts (human); 293T, immortalized embryonic kidney epithelial (human); HUVEC, human umbilical vein endothelial (human); 8988T pancreatic adenocarcinoma (human); SuDHL4, B cell lympohoma (human); MOLT-4, T cell acute lymphoblastic leukemia (human); $CD4^+$ and $CD8^+$, active primary T cells (mouse); Jurkat, immortalized T lymphocyte (human). **b**, Total oxPPP flux as determined by $^{14}CO_2$ emission in naïve mouse $CD8^+$ T cells (unstimulated and cultured with IL-7) and activated mouse $CD8^+$ T cells (day 4 post plate-bound αCD3/αCD28 stimulation and cultured with IL-2) (mean ± s.d., $n = 2$ for naïve, $n = 5$ for active). **c**, Fraction cellular NADPH from the oxPPP, malic enzyme 1 (ME1) and isocitrate dehydrogenase (IDH1) in naïve and activated $CD8^+$ T cells (mean ± s.d., $n = 3$) (for tracers, see Supplementary Fig. 10b,c). **d**, NADPH concentration and active hydride ^2H-labeling dose response to G6PDi-1 after 2 h ([1-^2H]-glucose tracer) ($n = 3$). **e**, G6PDi-1 blocks oxPPP flux as determined by $^{14}CO_2$ emission (mean ± s.d., $n = 5$). *P* value calculated using a two-tailed Student's *t*-test. **f**, $NADP^+$/NADPH shift in response to G6PDi-1 is rapidly reversible. Active $CD8^+$ T cells were pretreated with indicated media for 2 h, followed by incubation with final media for 2 h (mean ± s.d., $n = 3$). **g**, Absolute NADPH and $NADP^+$ pools after G6PDi-1 (2 h) ($n = 3$). **h**, Water-soluble metabolite in active $CD8^+$ T cells treated with G6PDi-1 (2 h) (mean, $n = 3$). Metabolites displaying a fold change of more than four are highlighted in red. **i**, Western blots of G6PD (combined endogenous and transgenic) in active $CD8^+$ T cells from G6PD overexpressing mice (G6PD-Tg mice). WT/WT, wild-type mice (no *G6PD* transgene expression); WT/Tg, heterozygous expression; Tg/Tg, homozygous expression. See Supplementary Fig. 16 for uncropped gels. Representative results of two independent experiments. **j**,**k**, Dose response to G6PDi-1 of NADPH (**j**) and $NADP^+$ (**k**) in active $CD8^+$ T cells from wild-type or G6PD-Tg mice ($n = 3$). Asterisks * and ** denote significant differences between WT/WT and Tg/Tg mice at each of the tested doses using a two-tailed unpaired Student's *t*-test. The following *P* values were obtained for NADPH levels: 5 μM, $P = 0.011$; 10 μM, $P < 0.0001$; 25 μM, $P = 0.019$; 50 μM, $P = 0.0010$. The following *P* values were obtained for $NADP^+$ levels: 5 μM, $P = 0.0011$; 10 μM, $P = 0.0012$; 25 μM, $P < 0.0001$; 50 μM, $P \leq 0.0001$.

Motivated by the need for an on-target tool compound to inhibit cellular G6PD, we engaged in substantial chemistry efforts. These led to the cell-active on-target G6PD inhibitor, G6PDi-1. We then used G6PDi-1 to better understand cellular NADPH homeostasis. While the oxPPP is often described as being the canonical, dominant pathway for producing cytosolic NADPH, few studies have directly tested this. As expected, RBCs, which lack mitochondria and therefore the required substrates for producing NADPH when

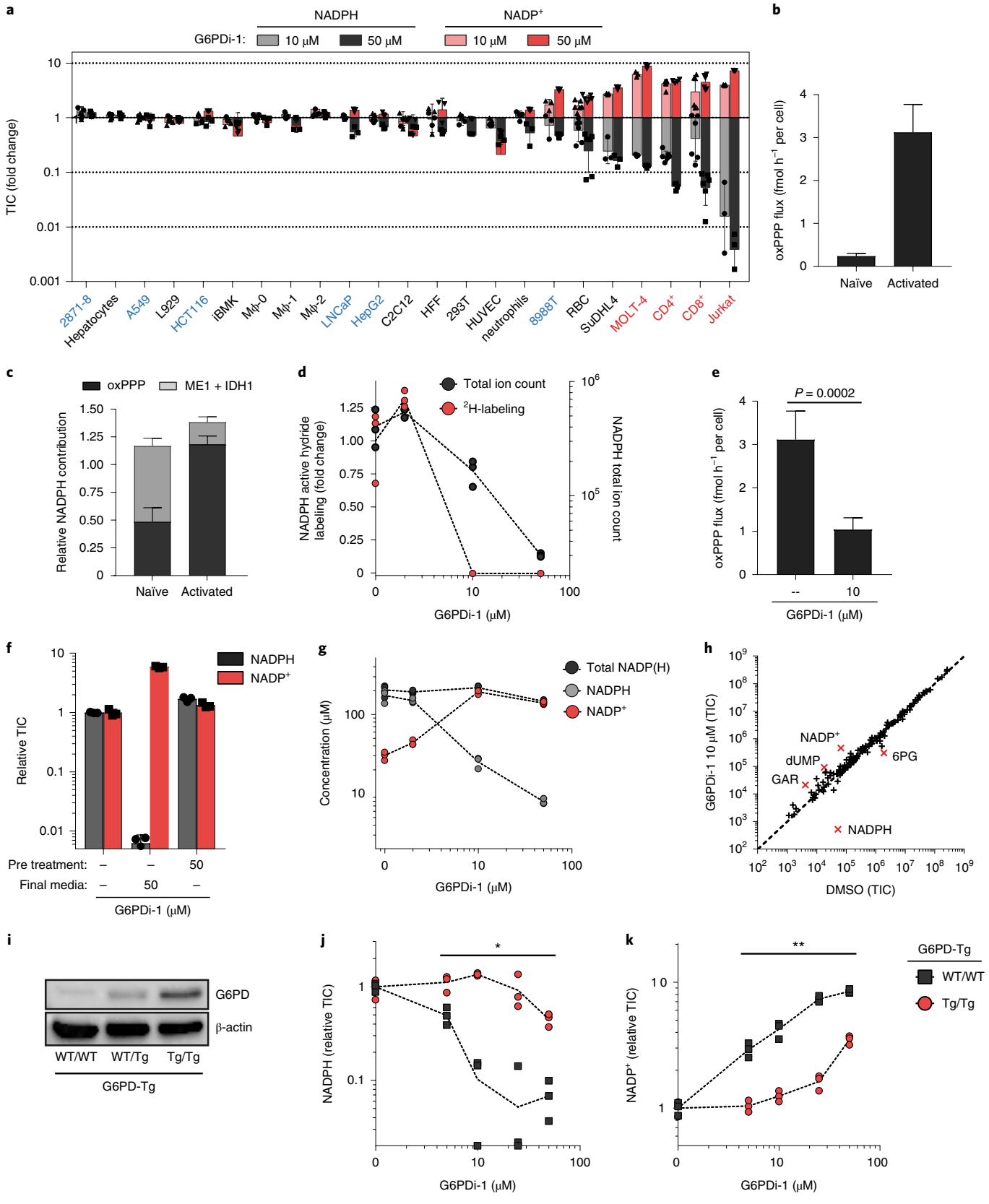

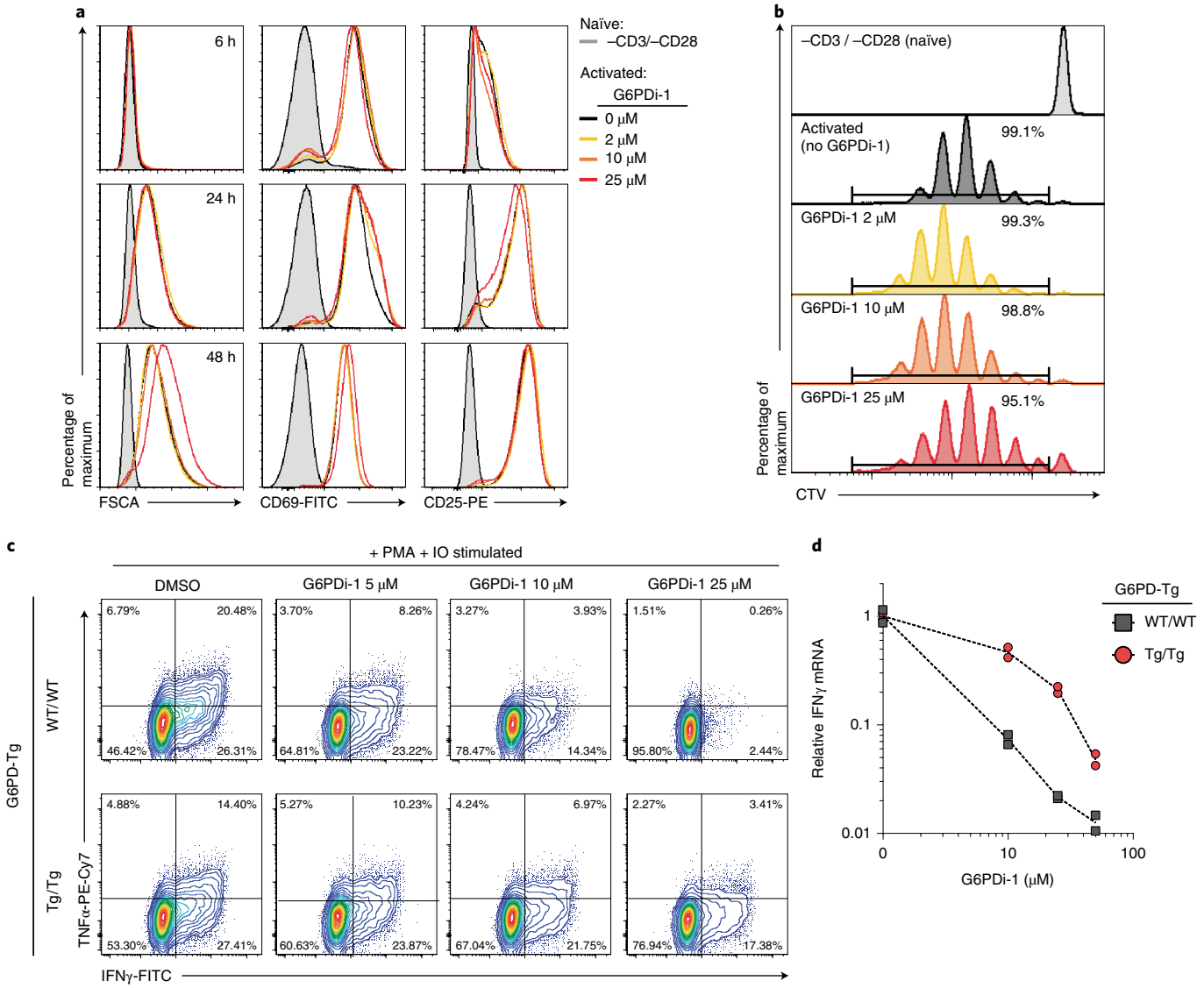

Fig. 4 | G6PDi-1 suppresses T cell cytokine production while having a minimal effect on initial activation or proliferation. a, Flow cytometry analysis of cell size (FSCA) and activation markers (CD69 and CD25) of mouse naïve CD8⁺ T cells either rested in naïve state or stimulated by CD3/CD28⁺ IL-2 in the presence of increasing concentrations of G6PDi-1. Representative results of two independent experiments. **b**, Proliferation of CD8⁺ T cells either rested in naïve state or stimulated by CD3/CD28⁺ IL-2 in the presence of increasing concentrations of G6PDi-1 at day 4 postactivation based on CellTrace Violet (CTV) dilution. Representative results of two independent experiments. **c**, Intracellular cytokines in active CD8⁺ T cells from wild-type or G6PD-Tg mice after a 6 h stimulation with PMA and ionomycin (IO) in the presence of the indicated dose of G6PDi-1. **c**,**d**, Representative results of two independent experiments. **d**, Corresponding *Ifng* mRNA in active CD8⁺ T cells from wild-type or G6PD-Tg mice (normalized to *Gapdh* expression and no G6PDi-1 control) ($n = 2$).

the oxPPP is blocked, showed decreased NADPH upon G6PDi-1 treatment. Many other cell lines were almost completely insensitive. Lymphocytes, however, including primary mouse active CD4⁺ and CD8⁺ T cells and human T-ALL cell lines, were yet more sensitive than RBCs. Consistent with this, we observed that activated T cells do not express substantial ME1 or IDH1, and make NADPH almost solely through the oxPPP, which is strongly upregulated during T cell activation.

If T cells are most sensitive to acute G6PD inhibition, why are clinical manifestations of G6PD deficiency most apparent in RBCs? Activated T cells, unlike mature RBCs, have intense biosynthetic requirements. Previous work has shown that biosynthesis—of proline, deoxyribonucleotides and especially fat—is a main consumer of cytosolic NADPH in proliferating mammalian cells[36]. But, evidence suggests RBCs in G6PD deficient patients are most often impaired through lower levels of enzyme, rather than reduced catalytic function[37]. Unlike T cells, mature RBCs are enucleated, and therefore unable to express new protein. As such, G6PD levels are gradually lost over the life span of RBCs (~120 d), with older RBCs retaining <10% of their original G6PD activity[38]. Mutations in G6PD accelerate this degradation[37]. Indeed, patients possessing G6PD variants with the lowest enzyme stability often experience the worst clinical outcomes[39]. Variants that reduce enzyme stability and thereby deplete G6PD activity in RBCs by >95% only modestly impair G6PD activity in leukocytes, often leading to no functional deficit[40,41]. This makes sense as, in their activated proliferating state, T cells are composed almost solely of freshly made protein. Severe G6PD mutations that affect enzyme catalytic ability (rather than protein stability) can present with immune deficiency[42].

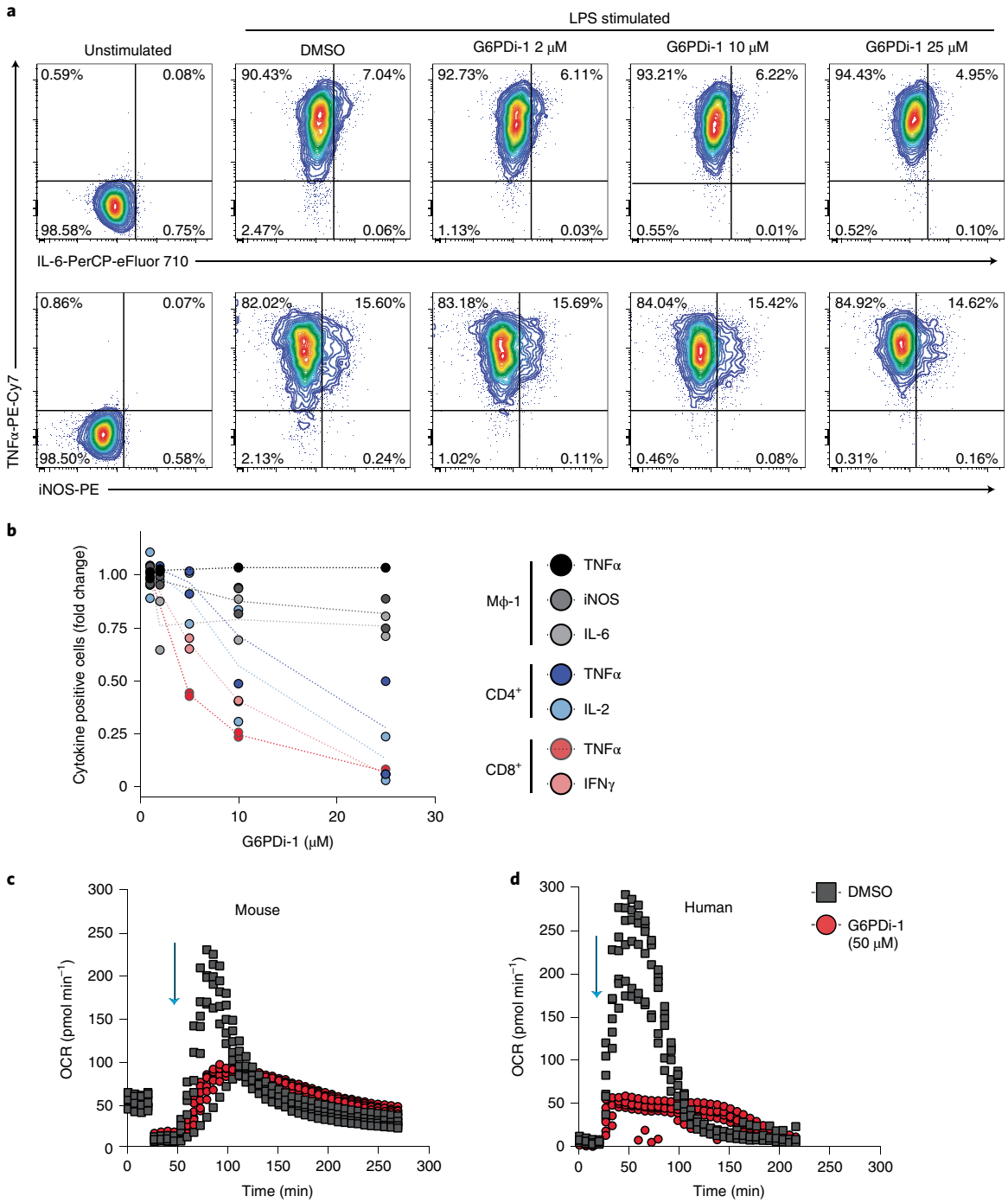

Fig. 5 | G6PDi-1 suppresses neutrophil oxidative burst. a, Intracellular cytokines in bone-marrow-derived macrophages after a 6 h stimulation with LPS and IFNγ in the presence of the indicated dose of G6PDi-1. Representative results of two independent experiments. **b**, Cytokine effects of G6PDi-1 across cell types ($n = 2$). **c**,**d**, Neutrophil oxidative burst as measured by the Seahorse Extracellular Flux Analyzer. OCR was monitored in mouse (**c**) and human (**d**) neutrophils that were activated with PMA (100 nM, indicated by blue arrows) in the presence of 50 μM G6PDi-1 or vehicle control ($n = 6$).

The inability of T cells to maintain NADPH homeostasis on G6PD blockade did not prevent initial activation or growth, but profoundly inhibited pro-inflammatory cytokine production. Similar cytokine effects were not observed in macrophages, which better maintained NADPH in the face of G6PDi-1. The mechanism linking G6PD to cytokine production remains unclear, but appears to involve defects in transcriptional activation. It is tempting to speculate that previous reports linking restriction of glycolysis—via GLUT1 knockdown, glucose depletion or glucose replacement with 2-deoxyglucose or galactose—with decreased cytokine secretion may be due to oxPPP blockade[43–47].

As expected, G6PD inhibition resulted in increased total cellular ROS. The general antioxidant *N*-acetyl-cysteine was able to block the increased ROS but did not restore cytokine secretion. This may reflect the complex role of ROS in immune cell activation, with the right amount required in the right subcellular location. Such a precise ROS control may make T cells uniquely sensitive both to glucose availability and to G6PD inhibition. Other immune cells may

also be sensitive to G6PD inhibition for other reasons, as shown here for neutrophils and oxidative burst.

Development of G6PD inhibitors with appropriate pharmacokinetic properties for in vivo studies is an important objective, and will help further elucidate the enzyme's immune and other roles. In the immediate future, we hope that G6PDi-1 will prove to be a valuable initial tool for exploring the biological role of G6PD across diverse cellular contexts.

Online content

Any Nature Research reporting summaries, source data, extended data, supplementary information, acknowledgements, peer review information; details of author contributions and competing interests; and statements of data and code availability are available at https://doi.org/10.1038/s41589-020-0533-x.

Received: 7 June 2019; Accepted: 27 March 2020;
Published online: 11 May 2020

References

1. Voet, D., Voet, J. G. & Pratt, C. W. *Fundamentals of Biochemistry: Life at the Molecular Level 5th edn* (Wiley, 2016).
2. Stanton, R. C. Glucose-6-phosphate dehydrogenase, NADPH, and cell survival. *IUBMB Life* **64**, 362–369 (2012).
3. Uhlen, M. et al. Proteomics. Tissue-based map of the human proteome. *Science* **347**, 1260419 (2015).
4. Kowalik, M. A., Columbano, A. & Perra, A. Emerging role of the pentose phosphate pathway in hepatocellular carcinoma. *Front. Oncol.* **7**, https://doi.org/10.3389/fonc.2017.00087 (2017).
5. Zhang, Q. et al. Overexpression of G6PD represents a potential prognostic factor in clear cell renal cell carcinoma. *J. Cancer* **8**, 665–673 (2017).
6. Nagashio, R. et al. Prognostic significance of G6PD expression and localization in lung adenocarcinoma. *Biochim. Biophys. Acta* **1867**, 38–46 (2019).
7. Pu, H. et al. Overexpression of G6PD is associated with high risks of recurrent metastasis and poor progression-free survival in primary breast carcinoma. *World J. Surgical Oncol.* **13**, 323–323 (2015).
8. Longo, L. et al. Maternally transmitted severe glucose 6-phosphate dehydrogenase deficiency is an embryonic lethal. *EMBO J.* **21**, 4229–4239 (2002).
9. Cappellini, M. D. & Fiorelli, G. Glucose-6-phosphate dehydrogenase deficiency. *Lancet* **371**, 64–74 (2008).
10. Chen, L. et al. NADPH production by the oxidative pentose-phosphate pathway supports folate metabolism. *Nat. Metabolism* **1**, 404–415 (2019).
11. Hamilton, N. M. et al. Novel steroid inhibitors of glucose 6-phosphate dehydrogenase. *J. Med. Chem.* **55**, 4431–4445 (2012).
12. Preuss, J. et al. Identification and characterization of novel human glucose-6-phosphate dehydrogenase inhibitors. *J. Biomol. Screening* **18**, 286–297 (2012).
13. Mele, L. et al. A new inhibitor of glucose-6-phosphate dehydrogenase blocks pentose phosphate pathway and suppresses malignant proliferation and metastasis in vivo. *Cell Death Dis.* **9**, 572 (2018).
14. Marks, P. A. & Banks, J. Inhibition of mammalian glucose-6-phosphate dehydrogenase by steroids. *Proc. Natl Acad. Sci. USA* **46**, 447–452 (1960).
15. Di Monaco, M. et al. Role of glucose-6-phosphate dehydrogenase inhibition in the antiproliferative effects of dehydroepiandrosterone on human breast cancer cells. *Brit. J. Cancer* **75**, 589–592 (1997).
16. Pashko, L. L., Lewbart, M. L. & Schwartz, A. G. Inhibition of 12-O-tetradecanoylphorbol-13-acetate-promoted skin tumor formation in mice by 16α-fluoro-5-androsten-17-one and its reversal by deoxyribonucleosides. *Carcinogenesis* **12**, 2189–2192 (1991).
17. Girón, R. A., Montaño, L. F., Escobar, M. L. & López-Marure, R. Dehydroepiandrosterone inhibits the proliferation and induces the death of HPV-positive and HPV-negative cervical cancer cells through an androgen- and estrogen-receptor independent mechanism. *FEBS J.* **276**, 5598–5609 (2009).
18. Ho, H. Y., Cheng, M. L., Chiu, H. Y., Weng, S. F. & Chiu, D. T. Dehydroepiandrosterone induces growth arrest of hepatoma cells via alteration of mitochondrial gene expression and function. *Int. J. Oncol.* **33**, 969–977 (2008).
19. Pacold, M. E. et al. A PHGDH inhibitor reveals coordination of serine synthesis and one-carbon unit fate. *Nat. Chem. Biol.* **12**, 452 (2016).
20. Mullarky, E. et al. Identification of a small molecule inhibitor of 3-phosphoglycerate dehydrogenase to target serine biosynthesis in cancers. *Proc. Natl Acad. Sci. USA* **113**, 1778 (2016).
21. Ducker, G. S. et al. Human SHMT inhibitors reveal defective glycine import as a targetable metabolic vulnerability of diffuse large B-cell lymphoma. *Proc. Natl Acad. Sci. USA* **114**, 11404–11409 (2017).
22. Lu, W., Wang, L., Chen, L., Hui, S. & Rabinowitz, J. D. Extraction and quantitation of nicotinamide adenine dinucleotide redox cofactors. *Antioxidant. Redox Signal.* **28**, 167–179 (2018).
23. Gordon, G., Mackow, M. C. & Levy, H. R. On the mechanism of interaction of steroids with human glucose 6-phosphate dehydrogenase. *Arch. Biochem. Biophys.* **318**, 25–29 (1995).
24. Zhang, Z., Chen, L., Liu, L., Su, X. & Rabinowitz, J. D. Chemical basis for deuterium labeling of fat and NADPH. *J. Am. Chem. Soc.* **139**, 14368–14371 (2017).
25. Mercaldi, G. F., Ranzani, A. T. & Cordeiro, A. T. Discovery of new uncompetitive inhibitors of glucose-6-phosphate dehydrogenase. *J. Biomol. Screening* **19**, 1362–1371 (2014).
26. Schafer, Z. T. et al. Antioxidant and oncogene rescue of metabolic defects caused by loss of matrix attachment. *Nature* **461**, 109–113 (2009).
27. Buck, M. D., O'Sullivan, D. & Pearce, E. L. T cell metabolism drives immunity. *J. Experimental Med.* **212**, 1345–1360 (2015).
28. Nobrega-Pereira, S. et al. G6PD protects from oxidative damage and improves healthspan in mice. *Nat. Commun.* **7**, 10894 (2016).
29. Ron-Harel, N. et al. Mitochondrial biogenesis and proteome remodeling promote one-carbon metabolism for T cell activation. *Cell Metab.* **24**, 104–117 (2016).
30. Geiger, R. et al. L-Arginine modulates T cell metabolism and enhances survival and anti-tumor activity. *Cell* **167**, 829–842.e813 (2016).
31. Sena, L. A. et al. Mitochondria are required for antigen-specific T cell activation through reactive oxygen species signaling. *Immunity* **38**, 225–236 (2013).
32. Padgett, L. E. & Tse, H. M. NADPH oxidase-derived superoxide provides a third signal for CD4 T cell effector responses. *J. Immunol.* **197**, 1733–1742 (2016).
33. Mak, T. W. et al. Glutathione primes T cell metabolism for inflammation. *Immunity* **46**, 675–689 (2017).
34. Nguyen, G. T., Green, E. R. & Mecsas, J. Neutrophils to the ROScue: mechanisms of NADPH oxidase activation and bacterial resistance. *Front. Cell Infect. Microbiol.* **7**, 373 (2017).
35. Goldfarb, A. H., McIntosh, M. K. & Boyer, B. T. Vitamin E attenuates myocardial oxidative stress induced by DHEA in rested and exercised rats. *J. Appl. Physiol.* **80**, 486–490 (1996).
36. Fan, J. et al. Quantitative flux analysis reveals folate-dependent NADPH production. *Nature* **510**, 298–302 (2014).
37. Morelli, A., Benatti, U., Gaetani, G. F. & De Flora, A. Biochemical mechanisms of glucose-6-phosphate dehydrogenase deficiency. *Proc. Natl Acad. Sci. USA* **75**, 1979–1983 (1978).
38. Marks, P. A., Johnson, A. B. & Hirschberg, E. Effect of age on the enzyme activity in erythrocytes. *Proc. Natl Acad. Sci. USA* **44**, 529–536 (1958).
39. Cunningham, A. D., Colavin, A., Huang, K. C. & Mochly-Rosen, D. Coupling between protein stability and catalytic activity determines pathogenicity of G6PD variants. *Cell Rep.* **18**, 2592–2599 (2017).
40. Morellini, M., Colonna-Romano, S., Meloni, T., Battistuzzi, G. & Gandini, E. Glucose-6-phosphate dehydrogenase of leukocyte subpopulations in normal and enzyme deficient individuals. *Haematologica* **70**, 390–395 (1985).
41. Ardati, K. O., Bajakian, K. M. & Tabbara, K. S. Effect of glucose-6-phosphate dehydrogenase deficiency on neutrophil function. *Acta Haematologica* **97**, 211–215 (1997).
42. Vives Corrons, J. L. et al. Severe-glucose-6-phosphate dehydrogenase (G6PD) deficiency associated with chronic hemolytic anemia, granulocyte dysfunction, and increased susceptibility to infections: description of a new molecular variant (G6PD Barcelona). *Blood* **59**, 428–434 (1982).
43. Macintyre, A. N. et al. The glucose transporter Glut1 is selectively essential for CD4 T cell activation and effector function. *Cell Metab.* **20**, 61–72 (2014).
44. Ho, P. C. et al. phosphoenolpyruvate is a metabolic checkpoint of anti-tumor T cell responses. *Cell* **162**, 1217–1228 (2015).
45. Cham, C. M. & Gajewski, T. F. Glucose availability regulates IFN-gamma production and p70S6 kinase activation in CD8+ effector T cells. *J. Immunol.* **174**, 4670–4677 (2005).
46. Shi, L. Z. et al. HIF1α–dependent glycolytic pathway orchestrates a metabolic checkpoint for the differentiation of TH17 and Treg cells. *J. Experimental Med.* **208**, 1367–1376 (2011).
47. Chang, C. H. et al. Posttranscriptional control of T cell effector function by aerobic glycolysis. *Cell* **153**, 1239–1251 (2013).

Methods

Cell lines, growth conditions and reagents. HCT116, HepG2, L929, LNCaP, A549, C2C12, HFF, 293T, MOLT-4, Jurkat and SuDHL4 cells were all originally obtained from ATCC. The 8988T cells were obtained from DSMZ and 71-8 cells and iBMK cells were a generous gift from E. White (Rutgers Cancer Institute of New Jersey). Pooled human umbilical vein endothelial cells were obtained from Thermo Fisher Scientific (no. C0155C) and were maintained in EBM-2 Basal Medium (CC-3156, Lonza) supplemented with EGM-2 SingleQuots Supplements (CC-4176, Lonza). All other adherent cell lines (unless otherwise specified) were maintained in DMEM (CellGro 10-017, Mediatech Inc.) supplemented with 10% fetal bovine serum (FBS) (F2442, Sigma Aldrich). All suspension cell lines (unless otherwise specified) were maintained in RPMI-1640 media supplemented with 10% FBS, 100 U ml^{-1} penicillin, 100 µg ml^{-1} streptomycin and 50 µM 2-mercaptoethanol. All cell lines were routinely screened for mycoplasma contamination. LentiCRISPR v.2 (52961) was obtained from Addgene. All primers were synthesized by Integrated DNA Technologies. Antibodies were used according to their manufacturer's directions. Anti-β-actin (5125) was obtained from Cell Signaling Technologies. Anti-G6PD (ab993); ME1 (ab97445) and IDH1 (EPR12296) were obtained from Abcam Inc. CoxIV antibody was obtained from Proteintech (11242-1-AP). Standard laboratory chemicals were from Sigma.

Chemical compounds. Synthetic procedures are provided in the Supplementary Note.

Oligonucleotides. For LentiCRISPR see Supplementary Table 1. For CRISPR–Cas9nickase see Supplementary Table 2. For PCR with reverse transcription see Supplementary Table 3.

G6PD protein expression. Partially truncated human G6PD (residues 28–515, Uniprot ID P11413) was subcloned into the pET28a vector using the Ndel and Xhol restriction enzyme sites and the following primers: 5′-agtcagcatatggtcagtcggatacacatattcatc-3′ and 5′-agtcagctcgagtcagagcttgtgggggttcac-3′. Recombinant G6PD was expressed in *Escherichia coli* BL21(De3)pLysS as an N-terminal His_6-tagged protein with an integrated thrombin cleavage site. Briefly, IPTG was added (final concentration of 1 mM) to induce protein expression when culture density reached an optical density (OD_{600}) of 0.6, followed by incubation at 37 °C overnight. Pellets were isolated and lysed by sonication in buffer containing 50 mM Tris (pH 8), 500 mM NaCl, 20 mM imidazole, 1 mM BME, 1 mM PMSF and 5% glycerol v/v. The lysate was centrifuged and filtered to remove insoluble debris. The resulting supernatant was fractionated twice with ammonium sulfate; first to 25% at 4 °C for 1 h, with the supernatant undergoing subsequent fractionation to 50% at 4 °C for 1 h. The precipitate was collected and dissolved in binding buffer consisting of 50 mM NaH_2PO_4, Tris (pH 8), 500 mM NaCl, 20 mM imidazole and 1 mM BME, and was loaded onto a Ni Sepharose HisTrap HP column (GE Healthcare, 17-5248-01). The column was washed with ~10 column volumes of binding buffer. Elution of G6PD was achieved with elution buffer consisting of 50 mM NaH_2PO_4, Tris (pH 8), 500 mM NaCl, 250 mM imidazole and 1 mM BME. The eluted protein was desalted and concentrated to remove the imidazole before undergoing thrombin cleavage using a Thrombin CleanCleave Kit (MilliporeSigma, C974M34). The tag-less protein was purified by size-exclusion chromatography using a Superdex 200 Increase 10/300 GL column (GE Healthcare) using buffer consisting of 50 mM Tris (pH 8), 150 mM NaCl and 1 mM BME. Eluted protein was concentrated using an Amicon Ultra 10 kDa MWCO filter (MilliporeSigma, UFC901008). Protein concentration was determined by Pierce BCA Assay (Thermo, 23225) and was stored in 10% glycerol at −80 °C.

G6PD enzymatic activity measurement by diaphorase-coupled assay. Inhibitor activity against recombinant human G6PD was determined using a resazurin-based diaphorase-coupled kinetic assay. Increasing doses of test compound in 96-well, opaque bottom plates were treated with assay buffer containing 50 mM triethanolamine pH 7.4, 1 mM $MgCl_2$, 0.1 mM resazurin, 0.03 mM $NADP^+$, 0.1 U ml^{-1} *Clostridium kluyveri* diaphorase (MilliporeSigma, D5540), 0.25 mg ml^{-1} bovine serum albumin and ~1 nM purified G6PD. The reaction was initiated by the addition of 1 mM glucose-6-phosphate (G6P). Plates were incubated at 30 °C and read every minute by a BioTek plate reader (Synergy HT) monitoring fluorescence emission at 590 nm following excitation at 530 nm. For Michaelis–Menten experiments $NADP^+$ and G6P concentrations were varied as indicated in figures. For jump dilution experiments, inhibitor was initially incubated in assay buffer containing ~10 nM G6PD for 30 min at 30 °C (1× dilution), before being diluted (1:50) into an equal volume of assay buffer without G6PD or inhibitor (50× dilution), followed by reaction initiation of both by the addition of 1 mM G6P. G6PD inhibition was determined by calculating the change in relative fluorescence over time (in relative fluorescence units per min) in the presence of different doses of test compound, followed by normalization against control wells without compound. GraphPad Prism (v.7.03) was used to perform a nonlinear curve fit (four-parameter) to determine IC_{50} values. Competitive and noncompetitive modes of G6PD binding by inhibitor were modeled using the built-in nonlinear regression analysis packages in Graphpad (v.8.2).

Generation of G6PD-null and hypomorphic PGD cell lines. Generation of clonal G6PD-null line in the HCT116 background have been previously described[10]. Using a similar approach, a clonal hypomorphic PGD cell line in the HCT116 background was generated. Briefly, paired-guide RNAs (*mPGD-1* and *mPGD-2*) against exon 3 of human *PGD* were cloned into plasmids containing Cas9 nickase expression vector and puromycin-resistant genes. Cells were transiently transfected with these plasmids using Lipofectamine 3000 (Life Technologies) and selected for 48 h with 2 µg ml^{-1} puromycin. After selection, cells were grown to confluence before single-cell plating in 96-well plates. Hypomorphic cell lines showed decreased but not ablated protein expression by western blotting.

Generation of batch G6PD-null cells in the HepG2 background was achieved using the lentiviral CRISPR–Cas9 vector system LentiCRISPR v.2 (Addgene no. 52961). Briefly, single-guide RNA sequences targeting exon-5 of human *G6PD* were designed using the crispr.mit.edu design tool. The identified protospacer adjacent motif sequences were subcloned into the LentiCRISPR v.2 using the BsmBI restriction endonuclease (NEB R0580S). Virus was produced through PEI (MilliporeSigma, 408727) transfection of vectors and lentiviral packaging plasmids psPax2 and VSVG in 293T cells. Medium containing lentivirus was collected after 2 d and filtered through a PES filter (0.22 µm, MilliporeSigma). HepG2 cells transfected with virus targeting noncoding control or *G6PD* and Polybrene (8 µg ml^{-1}, Invitrogen). Cells were split after 48 h into RPMI media (10% FBS) containing puromycin (2 µg ml^{-1}) and cultured for 3 d. G6PD knockout was confirmed by western blotting.

CETSA. Lysates from HepG2 cells at 75% confluence were isolated with 0.5% Triton in TBS (20 mM, Tris pH 7.4, 150 mM NaCl) for 30 min on ice, precleared by centrifugation and used for thermal shift assay as described[48]. Briefly, inhibitor or DMSO control was added to lysates at indicated concentration and incubated for 30 min on ice followed by 3 min heating at 47, 50, 53 and 56 °C in a thermal cycler. After heating, tubes were cooled at room temperature for 3 min and insoluble fraction removed by centrifugation at 17,000*g* for 20 min. The soluble fraction was separated by SDS–PAGE, transferred to a polyvinylidene difluoride membrane and immunoblotted using indicated antibodies at a dilution of 1:2,000. Blots were developed by chemiluminescence and imaged using a LI-COR C-DiGit Western Blot Scanner. Two independent experiments were performed. Signal intensity of proteins from immunoblots was quantified using Image Studio v.5.2 for C-DiGit Scanner, and bands were normalized to signal intensity of the 47 °C treated samples. Relative signal intensities were plotted as bar graph relative to the DMSO treated control.

G6PD enzymatic activity measurement by LC–MS. Inhibitor activity against recombinant human G6PD was determined by direct product monitoring by LC–MS. Test compounds at indicated doses were treated with assay buffer containing 50 mM triethanolamine pH 7.4, 1 mM $MgCl_2$, 0.30 mM $NADP^+$, 0.25 mg ml^{-1} bovine serum albumin and ~1 nM purified G6PD. The reaction was initiated by the addition of 1 mM G6P (or water for negative control condition). Aliquots of reaction mixture were collected at indicated time points and rapidly quenched by diluting (1:5) into methanol precooled on dry ice. The mixtures were centrifuged at 13,000*g* for 20 min at 4 °C, and the resulting supernatants were diluted (1:20) into 40:40:20 methanol:acetonitrile:water and analyzed by LC–MS.

Colony formation assay. In 24-well plates, HCT116 wild-type or Δ*G6PD* cells (~1,000 per well) were seeded in DMEM supplemented with 10% dFBS and indicated compounds (1 ml). Cells were incubated for 7 d, followed by media removal and staining with crystal violet solution (0.5% in 80:20 water:methanol) for 15 min. Cells were gently washed with water (3x) and air-dried prior to imaging.

Mice. For all experiements, 7–12-week-old mice were used. Wild-type C57BL/6 were purchased from either the Charles River or Harlan laboratories. The mice were on normal light cycle (8:00–20:00) and had free access to water and a standard chow diet. The G6PD-Tg mouse line was generated at the Spanish National Cancer Research Center at the Transgenic Mice core facility using a 20-kb human genomic DNA construct containing the entire *G6PD* gene, including 2.5 kb of upstream flanking sequence and 2.0 kb of downstream flanking sequence[28]. G6PD-Tg mice were bred and maintained in the facilities of the University of Valencia.

Isolation, culture and stimulation of naïve CD8$^+$ or CD4$^+$ T cells. To isolate naïve CD8$^+$ or CD4$^+$ T cells, spleens were harvested and single-cell suspensions prepared by manual disruption and passage through a 70-µm cell strainer in PBS supplemented with 0.5% BSA and 2 mM EDTA. After RBC lysis, naïve CD8$^+$ or CD4$^+$ T cells were purified by magnetic bead separation using commercially available kits following vendor instructions (naïve CD8a$^+$ T Cell Isolation Kit, mouse or naïve CD4$^+$ T Cell Isolation Kit, mouse, Miltenyi Biotec Inc.).

Cells were cultured in complete RPMI media (RPMI 1640, supplemented with 10% FBS, 100 U ml^{-1} penicillin, 100 µg ml^{-1} streptomycin and 55 µM 2-mercaptoethanol). Naïve T cells were either rested in complete RPMI media supplemented with recombinant IL-7 (50 U ml^{-1}) or stimulated for 48 h with plate-bound anti-CD3 (10 µg ml^{-1}) and anti-CD28 (5 µg ml^{-1}) in complete RPMI media supplemented with 100 µM alanine (to ensure proper activation[49]) and

recombinant IL-2 (100 U ml^{-1}). Activated T cells were maintained in complete RPMI media supplemented with recombinant IL-2 (100 U ml^{-1}). All experiments on 'active' T cells were performed at day 4–5 postactivation.

Isolation, culture and stimulation of bone-marrow-derived macrophages. Mouse bone-marrow monocyte/macrophage progenitors were isolated from femur and tibia and cultured in BMM media (DMEM supplemented with 10% FBS, 20% L929-conditioned media, 100 U ml^{-1} penicillin and 100 µg ml^{-1} streptomycin). Expression of CD11b and F4/80 was checked by flow cytometry after 6 d in culture. Mature macrophages were either maintained in BMM media (MΦ-0 macrophages) or stimulated overnight with LPS (100 ng ml^{-1}) + IFNγ (20 ng ml^{-1}) for MΦ-1 activation or IL-4 (20 ng ml^{-1}) for MΦ-2 activation.

Isolation and culture of primary mouse hepatocytes. Primary hepatocytes were isolated from C57Bl/6 mice by perfusion of the liver with liver perfusion medium (1×) (Thermo Fisher 17701038) followed by digestion with one bottle of collagenase/elastase (Worthington Biochemical LK002066) and DNase1 (Worthington Biochemical, LK003170) in Krebs Ringer Buffer with HEPES and 0.5 mM $CaCl_2$. Digested liver was minced in hepatocyte wash medium (Thermo Fisher 17704024), passed through a 70 µm strainer and centrifuged at 50*g*. Dead cells were removed by adding a 25% percoll solution, centrifuging at 120*g* and aspirating the supernatant. Primary hepatocytes were plated at 1.2 million cells per well in collagen coated six-well plates in prewarmed DMEM with 100 nM insulin, 100 nM dexamethasone and 1% Glutamax.

Isolation and culture of mouse erythrocytes. To isolate RBCs, mice were euthanized by cervical dislocation followed by collection of ~200 µl whole blood via cardiac puncture into tubes containing 7.5 µl heparin (1,000 USP per ml, H3393, Sigma Aldrich). The cells were incubated on ice for ~5 min, then centrifuged (5 min, 500 r.p.m., 4 °C) followed by aspiration of the serum and buffy coat layer. Cells were gently resuspended in PBS and then pelleted (5 min, 500 r.p.m., 4 °C) three times. Cells were then resuspended in RPMI media and used immediately for experiments.

Isolation, culture and stimulation of neutrophils. Murine neutrophils were isolated from 8–12-week-old C56BL/6 mice. Mice were euthanized by cervical dislocation, and bone-marrow cells were gathered from the femur and tibia within 30 min. Cell suspensions were passed through a 70-µm cell strainer. Neutrophils were prepared using a negative selection kit (EasySep Mouse Neutrophil Enrichment Kit, Stem Cell Technologies), following manufacturer instruction. Cells were cultured in RPMI-1640 media supplemented with 10% heat-inactivated FBS, 100 U ml^{-1} penicillin, 100 µg ml^{-1} streptomycin, 5 mM HEPES and 2 mM EDTA. To stimulate neutrophils, 100 nM phorbol 12-myristate 13-acetate (PMA) (Cayman Chemical) was added to the media.

Human neutrophils were isolated from 8 ml of blood collected from healthy donors. Neutrophils were purified using the MACSxpress Whole Blood Neutrophil Isolation Kit (Miltenyi Biotec 130-104-434) followed by erythrocyte depletion (Miltenyi Biotec 130-098-196) according to the manufacturer's instructions.

Neutrophil oxidative burst assay. Suspended neutrophils were plated in culture wells precoated with Cell-Tak (Corning), spun at 200*g* for 1 min with minimal acceleration/deceleration and then incubated for 1 h at 37 °C. Murine neutrophils were plated at 2×10^5 cells per well, in RPMI-1640 media (sodium bicarbonate withheld). Human neutrophils were plated at 5×10^4 cells per well, in RPMI-1640 media supplemented with 0.1% human serum albumin. Inhibitor (G6PDi-1, 50 µM) or vehicle control were added just before starting the assay. Mouse neutrophils were also treated with rotenone (0.5 µM, BioVision) + antimycin A (0.5 µM, BioVision) at $t = 20$ min. Oxidative burst was stimulated with PMA (100 nM, Cayman Chemical); OCR was measured using the XF-96e extracellular flux analyzer (Seahorse Bioscience).

Flow cytometry analysis. To analyze cell surface markers expression, cells were collected, washed with PBS and stained with the viability dye Live/Dead Aqua. Cells were then washed with staining buffer and stained for surface markers: CD4 (APC-Cy7, clone RM4-5,), CD8a (PerCP-Cy5.5, clone 53-6.7), CD25 (APC, clone PC61), CD44 (PE-Cy7, clone IM7), CD62L (PE, clone MEL-14) and CD69 (FITC, clone H1.2F3) for T cells and CD11b (APC, clone M1/70) and F4/80 (FITC, clone BM8) for macrophages.

To analyze proliferation, naïve CD8$^+$ T cells were stained with CTV dye and either maintained in a naïve state with IL-7 or stimulated with αCD3/αCD28$^+$ recombinant IL-2 in the presence of increasing concentrations of G6PDi-1. Cells were refed at days 2 and 3 poststimulation and proliferation measured at day 4 postactivation. Cells were collected, washed with staining buffered and stained with the viability dye propidium iodide.

To analyze intracellular cytokines, active T cells were re-stimulated with PMA (20 ng ml^{-1}) and ionomycin (1 µg ml^{-1}) in the presence of GolgiStop and increasing concentrations of G6PDi-1. After a 6 h incubation period, cells were collected, washed with PBS and stained with the viability dye Live/Dead Aqua. Cells were then washed with staining buffer and stained for surface markers: CD4 (APC-Cy7, clone RM4-5,), CD8a (PerCP-Cy5.5, clone 53-6.7). Cells were then fixed and permeabilized and stained for intracellular cytokines: IFNγ (FITC, clone XMG1.2), TNFα (PE-Cyanine7, clone MP6-XT22) and IL-2 (PE, clone JES6-5H4). To analyze intracellular cytokines, mature macrophages were stimulated with LPS (100 ng ml^{-1}) + IFNγ (20 ng ml^{-1}) in the presence of GolgiStop and increasing concentrations of G6PDi-1. After a 6 h incubation period, cells were collected, washed with PBS and stained with the viability dye Live/Dead Aqua. Cells were then fixed and permeabilized and stained for intracellular cytokines: TNFα (PE-Cyanine7, clone MP6-XT22) and IL-6 (PerCP-eFluor 710, clone MP5-20F3) and for iNOS (PE, clone CXNFT).

For measuring intracellular ROS levels, cells were incubated for 2 h in the presence of increasing concentrations of G6PDi-1 and then stained for ROS and viability using CellROX Green Flow Cytometry Assay Kit following the manufacturer's instructions. In some experiments, *N*-acetyl cysteine (1 mM), galactose oxidase (0.045 U ml^{-1}) + galactose (500 µM) or potassium superoxide (0.5 µg ml^{-1}) were added to the culture media at the same time the drug and/or PMA and ionomycin were added. All flow cytometry was analyzed with an LSR II (BDbiosciences) using standard filter sets and FCS express 7.01 flow cytometry software (De Novo Software). Gating strategies for flow cytometry analyses are shown in Supplementary Fig. 15.

T_{reg} assays. Spleen and peripheral lymph nodes were harvested and processed to single-cell suspensions of lymphocytes. RBCs were removed with hypotonic lysis. We used magnetic beads (Miltenyi Biotec) for isolation of conventional T cells (T_{conv}, CD4$^+$CD25$^-$), T_{reg} (CD4$^+$CD25$^+$) and antigen presenting cells (CD90.2$^-$). For cell culture medium, we used RPMI-1640 medium supplemented with 10% FBS, penicillin (100 U ml^{-1}), streptomycin (100 µg ml^{-1}) and 55 µM β-mercaptoethanol T_{reg} suppression and iT_{reg} polarization were conducted as previously reported[50]. For T_{reg} suppression assays, T_{conv} were purified and stimulated with irradiated antigen presenting cells plus CD3ε mAb (1 µg ml^{-1}, BD Pharmingen). To assess proliferation, T_{conv} cells were labeled with carboxyfluorescein succinimidyl ester and T_{reg} cells with CellTrace Violet. After 72 h, proliferation of T_{conv} and T_{reg} cells was determined by flow cytometric analysis of carboxyfluorescein succinimidyl ester and CellTrace Violet dilution, respectively. For conversion to Foxp3$^+$ T_{reg} cells, T_{conv} cells were incubated for 3–5 d with CD3ε/CD28 mAb beads, plus TGFβ (3 ng ml^{-1}) and IL-2 (25 U ml^{-1}), and analyzed by flow cytometry for Foxp3$^+$ iT_{reg}. Flow cytometry data was captured using Cytoflex (Beckman Coulter) and analyzed using the FlowJo v.10.2 software.

Absolute quantification of oxPPP flux using [1-^{14}C]-glucose and [6-^{14}C]-glucose. Glucose oxidation flux through oxPPP was determined from difference in the rate of $^{14}CO_2$ released from [1-^{14}C]-glucose and [6-^{14}C]-glucose, as previously described with some modification[51,52]. RPMI-1640 media without sodium bicarbonate was supplemented with 0.74 g l^{-1} of $NaHCO_3$, 2.5 mM HEPES pH 7.4, 10% dFBS and 1% of either [1-^{14}C]-glucose or [6-^{14}C]-glucose. Three million primary mouse naïve (rested in IL-7) or active CD8$^+$ T cells (in the presence of IL-2 and 0.1% DMSO or 10 µM G6PDi-1) were incubated for 4 h in a sealed 12.5-cm^2 flask. To facilitate the collection of $^{14}CO_2$, 100 µl of a 10 M KOH solution was introduced into the sealed flask using a center well for incubation flask (8823200000, DWK Life Sciences). The assay was stopped by injection of 1 ml 1 M HCL and the KOH solution then transferred to scintillation vials containing 10 ml scintillation solution for counting. The signal was corrected for the percentage of radioactive tracer in the medium. The oxPPP flux is calculated as follows:

$$\text{oxPPP flux}\left(\text{fmol h}^{-1}\ \text{cell}^{-1}\right) = \frac{^{14}CO_2\,(\text{nmol})}{\text{Cell number (M)} \times \text{labeling time (h)}} \times \frac{\text{Total glucose (nmol)}}{^{14}\text{C–glucose (nmol)}}$$

Tracer experiments. For all experiments involving stable isotope tracers (for example, [1-^{2}H]-glucose), the isotope tracer nutrient was substituted for unlabeled nutrient at the same concentration normally found in the base media for a given cell type (for example, DMEM for HCT116, RPMI for T cells and so on). In addition, dialyzed FBS was used as a supplement in place of FBS.

Cytosolic NADPH sources were traced, and redox-active hydride labeling was calculated, using a previously described strategy[10,24]. [1-^{2}H]-glucose (which directly traces G6PD) or [3-^{2}H]-glucose (which directly traces PGD) were used for tracing oxPPP contribution to NADPH; [4-^{2}H]glucose for ME1; [2,3,3,4,4-$^2H_5$]-glutamine, for both ME1 and IDH1 and D_2O, to account for solvent exchange.

The mass difference between $^{13}C_1$ and $^2H_1$ NADPH and NADP$^+$ cannot be resolved using the Q Exactive Plus. Therefore, the natural ^{13}C abundance was corrected from the raw data. The labeling of the redox-active hydrogen of NADPH (active H) and correction for solvent exchange were done as previously described[24]. [1-^{2}H]-glucose and [3-^{2}H]-glucose contributions were corrected by glucose-6-phosphate labeling, [4-^{2}H]-glucose by malate labeling and [2,3,3,4,4-$^2H_5$]-glutamine by the average of citrate and malate labeling. OxPPP contribution was calculated as the sum of the normalized active H labeling for [1-^{2}H]-glucose and [3-^{2}H]-glucose, and ME1 plus IDH1 as the sum of the normalized active H labeling for [4-^{2}H]-glucose and [2,3,3,4,4-$^2H_5$]-glutamine.

Metabolite extraction. For analysis of intracellular metabolites by LC–MS, adherent cell lines were plated and grown to 80% confluency in six-well plates. At the start of an experiment, the appropriate media was added to cells, which included isotope tracers and/or chemical inhibitors as described. Cells were incubated at 37 °C at 5% CO_2 for 2 h (unless otherwise noted). For all experiments involving small molecule agents, DMSO concentrations were <0.2%. After 2 h, media was removed by aspiration and metabolome extraction was performed (without any wash steps) by the addition of 800 µl of ice-cold solvent (40:40:20 acetonitrile:methanol:water + 0.5% formic acid). After a 1-min incubation on ice, the extract was neutralized by the addition of NH_4HCO_3 (15% w/v). The samples were incubated at −20 °C for ~30 min, at which point the wells were scraped and the extract transferred to Eppendorf tubes and centrifuged (15 min, 16,000 r.p.m., 4 °C). The resulting supernatant was frozen on dry ice and kept at −80 °C until LC–MS analysis.

For suspension cells (including T cells and RBCs), 2×10^6 cells were seeded in 1 ml of media in 12-well plates and incubated with appropriate media, which included isotope tracers and/or chemical inhibitors and/or cytokines as described. For all experiments involving small molecule agents, DMSO concentrations were <0.2%. After 2 h, cell suspensions were transferred to 1.5-ml tubes and pelleted (30 s, 6,000 r.p.m., room temperature). Media was removed by aspiration and metabolome extraction was performed by the addition of 75 µl of ice-cold solvent (40:40:20 ACN:MeOH:H_2O + 0.5% formic acid). After a 5 min incubation on ice, acid was neutralized by the addition of NH_4HCO_3. After centrifugation (15 min, 16,000 r.p.m., 4 °C), the resulting supernatant was transferred to a clean tube, frozen on dry ice and kept at −80 °C until LC–MS analysis. For neutrophil experiments, metabolites were extracted after 30 min of stimulation with PMA using similar extraction conditions.

LC–MS analysis. Unless otherwise noted, metabolites were analyzed using a quadrupole-orbitrap mass spectrometer (Q Exactive Plus, Thermo Fisher Scientific), coupled to hydrophilic interaction chromatography with LC separation on a XBridge BEH Amide column (Waters), or a stand-alone Orbitrap (Thermo Fisher Exactive) coupled to reversed-phase ion-pairing chromatography with LC separation on a HSS-T3 column (Waters). Both mass spectrometers were operating in negative ion mode and were coupled to their respective liquid chromatography methods via electrospray ionization. Detailed analytical conditions have been previously described[24,53]. Metabolites from neutrophils were analyzed using similar methods that have been previously described[54].

Adherent cell metabolite abundances were normalized by packed cell volume; suspension cells to cell count. Unless otherwise indicated, isotopic labeling of metabolites arising from incubation with ^{13}C or ^{2}H labeled nutrients were corrected for natural abundance, as previously described[55]. Data were analyzed using the ElMaven software (v.0.2.4, Elucidata), with compounds identified based on exact mass and retention time match to commercial standards. For metabolomics analysis, metabolite data were normalized to control condition and clustered using Cluster v.3.0 software. Heatmaps were plotted using Java Treeview.

Absolute quantification of $NADP^+$ and NADPH in active $CD8^+$ T cells. Active $CD8^+$ T cells were cultured and metabolome extraction was performed as previously described. Packed cell volume was measured using Midwest Scientific PCV cell counting tubes and estimated to be 1.5 µl per 2×10^6 cells. Cell extracts were spiked with 1.5 µl of $NADP^+$ 2.5 or 25 µM or NADPH 20 or 200 µM. Absolute concentration was calculated based on the increase in $NADP^+$ or NADPH signal in the spiked samples.

Statistics. Samples sizes are defined in each figure legend. Results for technical replicates are presented as mean ± s.d. or s.e.m. Statistical significance between conditions was calculated using Student's *t*-test (two-tailed) when comparing two groups and one-way analysis of variance followed by Dunnett's or Tukey's post hoc analysis when comparing more than two. All statistical calculations were performed using the software package GraphPad Prism (v.7.03 and v.8.2).

Ethics. We have complied with all relevant ethical regulations regarding the use of research animals and human research participants.

Unless otherwise specified, animal studies followed protocols approved by the Princeton University Institutional Animal Care and Use Committee (protocol number 2032-17). Mouse neutrophil studies followed protocols approved by the University of Wisconsin Institutional Animal Care and Use Committee (protocol number M006219). Mouse T_{reg} studies followed protocols approved by the Children's Hospital of Philadelphia Institutional Animal Care and Use Committees (protocol number 19–000561). G6PD-Tg mouse studies followed protocols approved by the University of Valencia Institutional Animal Care and Use Committee (protocol number A1444079171882).

Collection of blood from healthy donors followed the protocol approved by the University of Wisconsin Institutional Review Board (protocol number 2019-1031-CP001). Informed consent was obtained from all participants.

Reporting Summary. Further information on research design is available in the Nature Research Reporting Summary linked to this article.

Data availability

The data that support the findings of this study are available from the corresponding author upon reasonable request.

References

48. Martinez Molina, D. et al. Monitoring drug target engagement in cells and tissues using the cellular thermal shift assay. *Science* **341**, 84–87 (2013).
49. Ron-Harel, N. et al. T cell activation depends on extracellular alanine. *Cell Rep.* **28**, 3011–3021.e3014 (2019).
50. Xiao, H. et al. HDAC5 controls the functions of Foxp3(+) T-regulatory and CD8(+) T cells. *Internat. J. Cancer* **138**, 2477–2486 (2016).
51. Wang, R. et al. The transcription factor Myc controls metabolic reprogramming upon T lymphocyte activation. *Immunity* **35**, 871–882 (2011).
52. Katz, J. & Wood, H. G. The use of C14O2 yields from glucose-1- and -6-C14 for the evaluation of the pathways of glucose metabolism. *J. Biol. Chem.* **238**, 517–523 (1963).
53. Lu, W. et al. Metabolomic analysis via reversed-phase ion-pairing liquid chromatography coupled to a stand alone orbitrap mass spectrometer. *Anal. Chem.* **82**, 3212–3221 (2010).
54. Seim, G. L. et al. Two-stage metabolic remodelling in macrophages in response to lipopolysaccharide and interferon-γ stimulation. *Nat. Metabolism* **1**, 731–742 (2019).
55. Su, X., Lu, W. & Rabinowitz, J. D. Metabolite spectral accuracy on orbitraps. *Anal. Chem.* **89**, 5940–5948 (2017).

Acknowledgements

We thank C. DeCoste of the Princeton University flow cytometry resource facility and the Cytomics Unit of the IIS-La Fe for experimental set-up and design; R.S. O'Connor of University of Pennsylvania for assistance in setting up T cell experiments and for comments and suggestions on the figures; J. Jiao of the Children's Hospital of Philadelphia for technical assistance with the T_{reg} experiments; I. Babic of Nerdbio for assistance with the CETSA experiments; Y. Huang of Peking University for helpful suggestions pertaining to structure–activity relationship analysis and C. Bartman and the rest of members of the Rabinowitz laboratory for comments and suggestions. This work was supported by National Institutes of Health grant nos. 1DP1DK113643 and R01 CA163591. J.C.G.C. is supported by funding from the European Union's Horizon 2020 research and innovation program under the Marie Sklodowska-Curie grant agreement no. 751423.

Author contributions

J.D.R., J.M.G., J.C.G.-C. and H.K. conceived the study and designed the experiments. J.M.G. developed the in vitro and cell-based assays, conducted the biochemical characterization of G6PDi-1 and characterized the metabolic effects of G6PDi-1 HCT116, HepG2 and other adherent cell lines. J.C.G.C. characterized the metabolic effects of G6PDi-1 in suspension cell lines and the functional effects of G6PDi-1 in T cells and macrophages. J.W., E.S. and H.P. conducted protein expression and purification, in vitro activity assays and western blotting. L.C. isolated m*PGD* HCT116 cells. Z.Z. and T.T. isolated and cultured primary murine hepatocytes. U.H.B. designed and conducted the T_{reg} experiments. E.C.B. and J.F. designed and conducted the neutrophil experiments. M.C.G.-C. provided the G6PD transgenic mice. J.C.G.C., M.P.-N., M.C.G.-C. and A.L. designed and conducted the experiments with G6PD transgenic mice. H.K. and J.M.G. conducted the structure–activity relationship analysis. H.K. designed and oversaw the chemical synthetic strategy. J.D.R., J.M.G. and J.C.G.-C. wrote the paper. All authors edited and approved the manuscript.

Competing interests

Princeton University has filed a patent relating to the new G6PD inhibitors and their uses. J.D.R. is a cofounder of Raze Therapeutics, advisor and stock owner in Kadmon, Agios, CRP, LEAF and Bantam Pharmaceuticals and consultant to Pfizer. No competing interests were disclosed by the other authors.

Additional information

Supplementary information is available for this paper at https://doi.org/10.1038/s41589-020-0533-x.

Correspondence and requests for materials should be addressed to J.D.R.

Reprints and permissions information is available at www.nature.com/reprints.

nature research

Corresponding author(s): Joshua D. Rabinowitz

Last updated by author(s): Feb 26, 2020

Reporting Summary

Nature Research wishes to improve the reproducibility of the work that we publish. This form provides structure for consistency and transparency in reporting. For further information on Nature Research policies, see Authors & Referees and the Editorial Policy Checklist.

Statistics

For all statistical analyses, confirm that the following items are present in the figure legend, table legend, main text, or Methods section.

n/a	Confirmed	
☐	☒	The exact sample size (*n*) for each experimental group/condition, given as a discrete number and unit of measurement
☐	☒	A statement on whether measurements were taken from distinct samples or whether the same sample was measured repeatedly
☐	☒	The statistical test(s) used AND whether they are one- or two-sided *Only common tests should be described solely by name; describe more complex techniques in the Methods section.*
☒	☐	A description of all covariates tested
☒	☐	A description of any assumptions or corrections, such as tests of normality and adjustment for multiple comparisons
☐	☒	A full description of the statistical parameters including central tendency (e.g. means) or other basic estimates (e.g. regression coefficient) AND variation (e.g. standard deviation) or associated estimates of uncertainty (e.g. confidence intervals)
☐	☒	For null hypothesis testing, the test statistic (e.g. *F*, *t*, *r*) with confidence intervals, effect sizes, degrees of freedom and *P* value noted *Give P values as exact values whenever suitable.*
☒	☐	For Bayesian analysis, information on the choice of priors and Markov chain Monte Carlo settings
☒	☐	For hierarchical and complex designs, identification of the appropriate level for tests and full reporting of outcomes
☒	☐	Estimates of effect sizes (e.g. Cohen's *d*, Pearson's *r*), indicating how they were calculated

Our web collection on statistics for biologists contains articles on many of the points above.

Software and code

Policy information about availability of computer code

Data collection	Flow citometry data was collected using BD FACSDiva software. LC-MS data was collected using XCalibur software.
Data analysis	FCS express 7.01 flow cytometry software (De Novo Software) and FlowJo 10.2 software for flow citometry data. ElMAVEN (v0.2.4, Elucidata) was used for LC-MS data analysis. For heatmap representations data were clustered using Cluster 3.0 software and heatmaps were plotted using Java Treeview 1.1.6r4 All graphing and associated statistical analysis was performed using GraphPad Prism 7.03 and 8.02 R code for correction of natural 13C abundance was previously described in ref. 56 Matlab code for calculation of active hydride labeling was previously described in ref. 24

For manuscripts utilizing custom algorithms or software that are central to the research but not yet described in published literature, software must be made available to editors/reviewers. We strongly encourage code deposition in a community repository (e.g. GitHub). See the Nature Research guidelines for submitting code & software for further information.

Data

Policy information about availability of data

All manuscripts must include a data availability statement. This statement should provide the following information, where applicable:

- Accession codes, unique identifiers, or web links for publicly available datasets
- A list of figures that have associated raw data
- A description of any restrictions on data availability

The data that support the findings of this study are available from the corresponding author upon reasonable request.

Field-specific reporting

Please select the one below that is the best fit for your research. If you are not sure, read the appropriate sections before making your selection.

☒ Life sciences ☐ Behavioural & social sciences ☐ Ecological, evolutionary & environmental sciences

For a reference copy of the document with all sections, see nature.com/documents/nr-reporting-summary-flat.pdf

Life sciences study design

All studies must disclose on these points even when the disclosure is negative.

Sample size	No statistical methods were used to predetermine sample size for experimentation given the minimal experimental variation in in vitro and cell-based assays based on our previous experience.
Data exclusions	No data were excluded from the analysis.
Replication	In most of the experiments at least 3 technical replicates were used and data usually shows one experiment that is representative or at least 2 independent experiments. All the attempts of replication were succesful.
Randomization	Because all cells used for analysis were from the same inbred strain of mouse or from the same initial stock in the case of cell lines, no randomization was performed.
Blinding	No blinding was performed. Blinding was unnecessary as all data collection and analysis is quantitative and not qualitative in nature.

Reporting for specific materials, systems and methods

We require information from authors about some types of materials, experimental systems and methods used in many studies. Here, indicate whether each material, system or method listed is relevant to your study. If you are not sure if a list item applies to your research, read the appropriate section before selecting a response.

Materials & experimental systems

n/a	Involved in the study
☐	☒ Antibodies
☐	☒ Eukaryotic cell lines
☒	☐ Palaeontology
☐	☒ Animals and other organisms
☐	☒ Human research participants
☒	☐ Clinical data

Methods

n/a	Involved in the study
☒	☐ ChIP-seq
☐	☒ Flow cytometry
☒	☐ MRI-based neuroimaging

Antibodies

Antibodies used

IL-2; Rat anti-Mouse; PE; Clone: JES6-5H4; Catalog number: 554428; Vendor: BD Biosciences; Lot number: 8264745; dilution 1:50
IL-6; Rat anti-Mouse; PerCP-eFluor 710; clone MP5-20F3; Catalog number: 46-7061-80; Vendor: ThermoFischer Scientific; Lot number: 8264745; dilution 1:50
IFN-γ; Rat anti-Mouse; FITC; Clone: XMG1.2; Catalog number: 554411; Vendor: BD Biosciences; Lot number: 8099787; dilution 1:50
CD69; Hamster anti-Mouse; FITC; Clone: H1.2F3; Catalog number: 557392; Vendor: BD Biosciences; Lot number: 7339715; dilution 1:50
CD62L; Rat anti-Mouse; PE; Clone: MEL-14; Catalog number: 561918; Vendor: BD Biosciences; Lot number: 7111838; dilution 1:50
CD44; Rat anti-Mouse; PE-Cy7; Clone: IM7; Catalog number: 560569; Vendor: BD Biosciences; Lot number: 7188583; dilution 1:50
CD25; Rat anti-Mouse; APC; Clone: PC61; Catalog number: 561048; Vendor: BD Biosciences; Lot number: 7311638; dilution 1:50
CD8a; Rat anti-Mouse; PerCP-Cy5.5; Clone: 53-6.7; Catalog number: 551162; Vendor: BD Biosciences; Lot number: 7326606; dilution 1:50
CD4; Rat Anti-Mouse; APC-Cy7; Clone RM4-5; Catalog number: 565650; Vendor: BD Biosciences; Lot number: 8201958; dilution 1:50
CD11b; Rat anti-Mouse; FITC; Clone: M1/70; Catalog number: 557396; Vendor: BD Pharmigen; Lot number: 8295811; dilution 1:50
iNOS; Rat anti-Mouse; PE; clone CXNFT; Catalog number: 12-5920-80; Vendor: ThermoFischer Scientific; Lot number: 1978214; dilution 1:50
F4/80; Rat anti-Mouse; eFluor450; Clone: BM8; Catalog number: 48-4801-82; Vendor: Invitrogen; Lot number: 2055827; dilution 1:50
TNF alpha; Rat anti-Mouse; PE-Cyanine7; Clone: MP6-XT22; Catalog number: 25732180; Vendor: Invitrogen; Lot number:

8264745; dilution 1:50
CD4; Rat Anti-Mouse; Pacific blue; Clone: RM4-5; Catalog number: 558107; Vendor: BD Bioscience ; Lot number: 6245596; dilution 1:40
CD4; Rat Anti-Mouse; APC; Clone: GK1.5; Catalog number: 17-0041-83; Vendor: eBioscience ; Lot number: 4285738; dilution 1:40
Foxp3; Rat Anti-Mouse;eFluor®660; Clone: FJK16s; Catalog number: 50-5773-82; Vendor: eBioscience; Lot number: 4285738; dilution 1:10
Anti-G6PD; Rabbit anti-Mouse, Rat, Human; Clone: Polyclonal; Catalog number: ab993; Vendor: Abcam; Lot#: GR274589-34; dilution 1:1000
Anti-CoxIV ; Rabbit anti-Mouse, Rat, Human, Swine; Clone: Polyclonal; Catalog number: 11242-1-AP; Vendor: Proteintech; Lot#: 48768; dilution 1:5000
Anti-β-actin; Rabbit anti-Mouse, Rat, Human, Monkey, Bovine, Pig; Clone: Polyclonal; Catalog number: 4970; Vendor: Cell Signaling Technologies; Lot number: 14; dilution 1:1000
Anti-ME1; Rabbit anti-Mouse, Rat, Human; Clone: Polyclonal; Catalog number: ab97445; Vendor: Abcam; Lot number: GR176483-26; dilution 1:1000
Anti-IDH1; Rabbit anti-Mouse, Rat, Human; Clone: EPR12296; Catalog number: ab172964; Vendor: Abcam; Lot number: GR130705-6; dilution 1:1000
Anti-rabbit IgG, HRP-linked Antibody; Goat anti-rabbit; Clone: Polyclonal; Catalog number: 7074; Vendor: Cell Signaling Technologies; Lot number: 28; dilution 1:5000

Validation

We followed standard procedures and all antibodies listed have been used by a large number of laboratories and each antibody is validated by the company of purchase. The information can be accessed through the vendor webpage using the provided catalog numbers.

Eukaryotic cell lines

Policy information about cell lines

Cell line source(s)

HCT116, HepG2, L929, LNCap, A549, C2C12, HFF, 293T, MOLT-4, Jurkat, and SuDHL4 (ATCC).
8988T (DSMZ).
2871-8, and iBMK - gift from Dr. Eileen White (Rutgers Cancer Institute of New Jersey, New Brunswick, NJ).
HUVECs (ThermoFisher Scientific).

Authentication

No cell line authentication performed.

Mycoplasma contamination

All cell lines tested negative for mycoplasma.

Commonly misidentified lines
(See ICLAC register)

The cell lines used here are not listed in the ICLAC database.

Animals and other organisms

Policy information about studies involving animals; ARRIVE guidelines recommended for reporting animal research

Laboratory animals

Mus musculus, C57BL/6, male , 7-12 weeks old.

Wild animals

The study did not involve wild animals

Field-collected samples

The study did not involve field-collected samples

Ethics oversight

Unless otherwise specified, animal studies followed protocols approved by the Princeton University Institutional Animal Care and Use Committee (protocol number 2032-17). Mouse neutrophil studies followed protocols approved by the University of Wisconsin Institutional Animal Care and Use Committee (protocol number M006219). Mouse Treg studies followed protcols approved by the Children's Hospital of Philadelphia Institutional Animal Care and Use Committees (protocol number 13–000561). G6PD-Tg mouse studies followed protocols approved by the University of Valencia Institutional Animal Care and Use Committee (protocol number A1444079171882).

Note that full information on the approval of the study protocol must also be provided in the manuscript.

Human research participants

Policy information about studies involving human research participants

Population characteristics

Our protocol for human neutrophil studies recruits healthy adult volunteers of mixed gender and ethnicities for blood donation and neutrophil isolation.

Recruitment

Volunteers are generally recruited via email distribution. Given the nature of these experiments, there is a low likelihood of a self-selection bias impacting these results.

Ethics oversight

This work followed a protocol approved by the University of Wisconsin Institutional Review Board (Protocol number 2019-1031-CP001)

Note that full information on the approval of the study protocol must also be provided in the manuscript.

Flow Cytometry

Plots

Confirm that:

☒ The axis labels state the marker and fluorochrome used (e.g. CD4-FITC).

☒ The axis scales are clearly visible. Include numbers along axes only for bottom left plot of group (a 'group' is an analysis of identical markers).

☒ All plots are contour plots with outliers or pseudocolor plots.

☒ A numerical value for number of cells or percentage (with statistics) is provided.

Methodology

Sample preparation	For surface markers analysis: cells were harvested, washed at least once with PBS, incubated for 15min at RT with L/D aqua, and stained with antibodies targeting surface antigens in 2%FBS 1mM EDTA in PBS (staining buffer) for 30 minutes on ice and finally washed once with staining buffer. For analysis of intracellular cytokine/protein staining, cells were then fixed and permeabilized with fixation/ permeabilization solution (BD Cytofix/Cytoperm Cat#554714) at 4C for 20 minutes. Cells were then washed three times with 1X permeabilization buffer and stained for intracellular antigens for 30 min on ice in 1X permeabilization buffer. Cells were then washed two times before proceeding to cytometry analysis. For analysis of CTV-labeled cells, cells were harvested, washed at least once with staining buffer, and then stained for 15min in staining buffer containing PI.
Instrument	LSR II (BDbiosciences) and Cytoflex (Beckman Coulter)
Software	Data was acquired using BD FACSDiva software and processed using FCS express 6 flow cytometry software (De Novo Software). or FlowJo 10.2 software.
Cell population abundance	Purity of magnetic bead naive CD4+ or CD8+ T cell isolation was determined by flow cytometry with >90% naive CD4/CD8 expressing cells used for all experiments.
Gating strategy	For experiments measuring surface markers or intracellular cytokines in CD4+/CD8+ T cells: FSC-A, SSC-A live cells >> FSC-H, FSC-A singlets >> L/D aqua neg >> CD4-CD8+ For experiments measuring proliferation by CTV in CD8+ T cells: FSC-A, SSC-A live cells >> FSC-H, FSC-A singlets >> PI neg For experiments measuring intracellular cytokines/proteins in Macrophages: FSC-A, SSC-A live cells >> FSC-H, FSC-A singlets >> L/D aqua neg >> CD11b+F4/80+

☒ Tick this box to confirm that a figure exemplifying the gating strategy is provided in the Supplementary Information.